Review

Regolith-hosted Rare Earth Element Mineralization in the Esperance Region, Western Australia: Major Characteristics and Potential Controls

Nikita Sergeev * and Tiffany Collins

Posted Date: 14 August 2024

doi: 10.20944/preprints202408.1070.v1

Keywords: rare earth element; regolith deposit; weathering; ion-adsorption; groundwater; supergene enrichment; ionic clay; Western Australia; saprolite; arid climate

Review

Regolith-hosted Rare Earth Element Mineralization in the Esperance Region, Western Australia: Major Characteristics and Potential Controls

Nikita Sergeev [1,*] and Tiffany Collins [2]

[1] ERM Group Pty Ltd., Perth, Australia
[2] Northern Star Resources Ltd., Australia
* Correspondence: nikita.sergeev@erm.com

Abstract: A number of regolith-hosted REE occurrences have recently been discovered in the Esperance region in southern Western Australia. This paper summarizes major characteristics of the REE mineralization and discusses contributing factors and potential controls. The main aim is to explain why there is a lack of highly sought-after ion-adsorption clay type REE deposits across the region despite the presence of the regolith-hosted REE mineralization on a regional scale. Local mineralization mostly occurs as continuous flat-lying enrichment "blankets" within the residual regolith developed over Archaean–Proterozoic granite gneisses and granitoids with elevated REE content. The enriched horizon is commonly located in the lower saprolite and saprock and is accompanied by an overlying REE-depleted zone. This distribution pattern, together with the data on HREE fractionation and the presence of the supergene REE minerals, indicate chemogenic type enrichment formed by supergene REE mobilization into groundwater, downward transport and accumulation in the lower part of the weathering profile. Residual REE accumulation processes due to bulk rock volume and mass reduction during weathering also contribute to mineralization. It is proposed that climate and groundwater chemistry are the critical regional controls on the distribution of REEs in the weathering profile and on their speciation in the enrichment zone. Cenozoic aridification of climate in southwest Australia heavily overprinted pre-existing REE distributions in the weathering profile. Acidic (pH <4), highly saline groundwaters intensely leached away any relatively weakly bound, adsorbed or colloidal REE forms, moving them downward. Dissolved REEs precipitated as secondary phosphates in neutral to alkaline environment at lower Eh near the base of the weathering profile forming the supergene enrichment zone. Low denudation rates, characteristic of areas of low relief under the arid climate, are favourable for the preservation of the existing weathering profiles with REE mineralization.

Keywords: rare earth element; regolith deposit; weathering; ion-adsorption; groundwater; supergene enrichment; ionic clay; Western Australia; saprolite, arid climate

1. Introduction

As the global demand for rare earth elements (REEs) increases with the accelerating development of environmentally sustainable technologies, especially with regard to the energy transition (e.g., wind turbines, electric vehicles, energy-effective lighting, and solar panels), efforts are underway to find new resources for these critical elements [1–4]. Existing REE resources are vulnerable to supply disruption as production and refining capacity is centered around a small number of producing countries [5,6]. Consequently, the number of REE exploration projects and processing plants have been increasing in the recent years [4].

Ion-adsorption clay (IAC) deposits, the most sought-after type of the regolith-hosted REE mineralization, are a valuable source of REEs – although their input to the total resource is less than 4%, they account for over 80% of the global heavy rare earth element (HREE) supplies [4]. Most deposits are in southern China and Myanmar although there are several large deposits and active projects in Brazil and Africa, and a number of prospects in other countries.

 doi:10.20944/preprints202408.1070.v1

Regolith-hosted REE deposits are new to Australia, although the Newmont prospect in Western Australia was discovered in 2011. With the recent increasing demand for REEs, active exploration for the IAC-style deposits within Australia started three years ago with a number of projects actively explored to date. Presently, the Esperance region in South-Western Australia is the largest exploration hub with active exploration over an area about 200 km long and 120 km wide (Figure 1). Cowalinya, Salazar, Splinter Rock and Circle Valley deposits have been established there with Mineral Resources ranging from 98 to 344 Mt of ore at 870-1308 ppm Total REE Oxide (TREO) (Table 1).

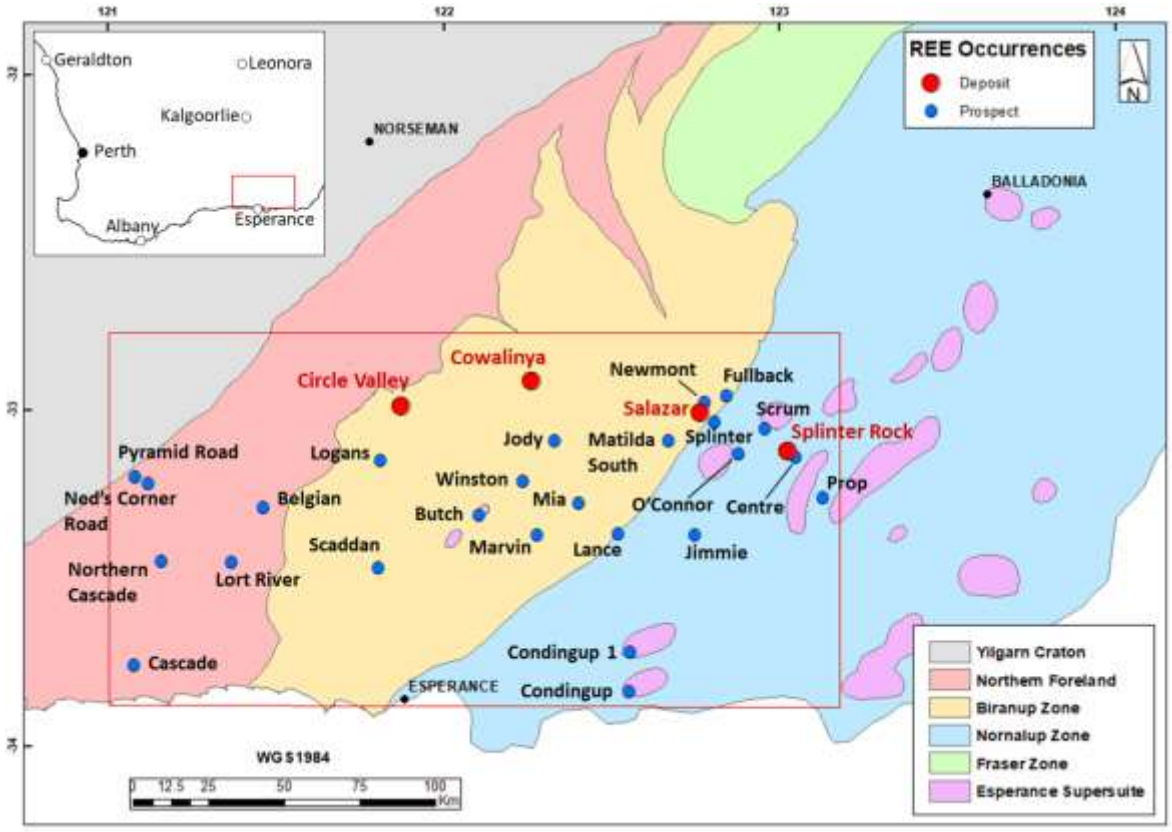

Figure 1. Simplified geological map of the Albany-Fraser Orogen and southern Yilgarn Craton showing the area actively exploring for REE in the Esperance region (red frame) and major REE occurrences. The geological map modified after [7].

Table 1. Mineral Resources of the regolith-hosted REE deposits in the Esperance region.

Deposit	Resource (Mt Ore)	TREO (ppm)	TREO (Kt)	Date	Mining Company	Reference
Cowalinya	159	870	138.33	3/10/2023	Heavy Rare Earths Ltd.	[8]
Salazar	190	1172	222.68	9/08/2023	West Cobar Metals	[9]
Splinter Rock	344	1308	449.952	18/07/2023	OD6 Metals	[10]
Circle Valley	98	890	87.22	14/06/2023	Meeka Metals	[11]

Despite several sizable resources discovered in the region, most projects hit the problem of a low recovery rate of the most sought-after ion-exchangeable REE component that is characteristic of IAC deposits. This form of REE is weakly bound by physical adsorption onto kaolinite and halloysite particles in clays and can be easily and cost-effectively extracted by traditional ionic leach reagents (ammonium or magnesium sulphate) at pH 4-5 and ambient temperatures. In most well-established IAC deposits in China ion-exchangeable REEs make over 60% of the total REE balance [12]. In contrast, reported recovery rates of ionic leachable REEs across the Esperance region are very low,

 doi:10.20944/preprints202408.1070.v1

commonly less than 2%: [13–15]. Leaching by relatively strong hydrochloric or sulfuric acid at pH 1-2, preferably at higher temperatures and for a long duration was found to be required for bulk REE recovery [16–18]. These issues significantly increase processing costs, and also add the problem of increased extraction of impurities by strong acids, which requires additional processing.

Our study aims to gaining more insight into this new-to-Australia REE mineralization style. As exploration and development of most projects is at early stages, only few research publications [15,19,20] are available to date and existing information is mostly limited to mining company reports and media releases.

This paper synthesizes the results of our research work with information available from open sources and aims to explain why there is a lack of the well sought-after IAC type deposits across the region despite the presence of the regolith-hosted REE mineralization on a regional scale. The study summarizes the major characteristics of local mineralization and discusses contributing factors and potential controls.

The weathering-related REE deposits have been previously variously termed ion-adsorption clay REE, clay-hosted REE, or weathered crust elution-deposited REE deposits. As the Esperance REE occurrences are mostly hosted by lower saprolite with relatively low clay content, the general term of regolith-hosted REE deposits is used for this study.

2. Materials and Methods

Twelve samples of mineralized regolith were collected from two drill holes (SAC021 and SAC059) at the Newmont and Splinter prospects. The samples were analyzed using sequential extraction following a generic five-step method, with separate ion-exchangeable and adsorbed fractions based on the methods of Shuman [21], Hall et al. [22] and Du et al. [23]. Each step represents further treatment of the initial 5 g sample (Table 2).

Prior to extraction, samples were not air or oven dried to retain the water-soluble fraction. Two subsamples (21-2 and 59-1) were oven dried at 40°C overnight to estimate potential water input. Organic-matter and sulfide fractions commonly estimated by the method [22] were not analyzed as the majority of the sulfides are associated with pyrite and organic matter concentrations are negligible at depths over 8 m. These fractions were incorporated into the amorphous and crystalline Fe oxyhydroxide bound fractions.

Fusion beads were made using 0.1000 ± 0.0002 g finely ground sample and 0.7000 ± 0.0002 g Norrish flux (lithium metaborate/lithium tetraborate). A certified reference material, Oreas 43P by Ore Research & Exploration Pty Ltd., Australia was prepared with the other samples to check fusion accuracy.

The supernatant solutions were analyzed using ICP-MS by TSW Analytical Pty Ltd. in Bibra Lake, Western Australia using an Agilent 7700 quadrupole ICP-MS system. The ICP-MS detection limits were 0.3 ppb for REE (including Y) and 0.1 ppm for Fe and Mn.

Blank solutions with no sample were included in the sequential extraction workflow to ensure no contamination occurred. These solutions contained $<1.9\times10^{-4}$ mg/kg total REE (TREE) for all fractions except the residual, which had less than 2.0×10-3 mg/kg TREE demonstrating good accuracy of the method.

Table 2. Sequential extraction procedure (modified after [21–23]. Each step represents further treatment of the initial 5 g sample.

Extraction Step	Procedure
1. Water soluble and ion-exchangeable	To 5 g of sample add 20 mL of 1.0 M $Mg(NO_3)_2$. Shake for 2 h. Centrifuge 15 min at 3000 rpm. Decant supernatant solution and rinse residue with 5 mL H_2O twice. Add rinses to supernatant and analyze.
2. Adsorbed and carbonate-bound	To a 1 g derivative from the previous step, add 20 mL of 1.0 M CH_3COONa (adjusted to pH 5 using CH_3COOH). Shake for 6 hrs. Centrifuge for 15 min at 3000 rpm. Decant supernatant solution and rinse residue with 5 mL H_2O twice. Add rinses to supernatant and analyze.

 doi:10.20944/preprints202408.1070.v1

3. Amorphous Fe oxyhydroxide bound	To the residue from the previous step add 20 mL of 0.25 M $NH_2OH{\cdot}HCl$ in 0.25 M HCl. Vortex for 5-10 sec. Place in a water bath at 60°C for 2 hrs. Centrifuge for 15 min at 3000 rpm. Decant supernatant solution and rinse residue with 5 mL H_2O twice. Add rinses to supernatant and analyze.
4. Crystalline Fe oxyhydroxide bound	To the residue from the previous step, add 30 mL of 0.25 M $NH_2OH{\cdot}HCl$ in 25% CH_3COOH. Cap and vortex for 5-10 sec. Place in a water bath at 90°C for 3 hrs. Centrifuge for 15 min and decant the supernatant liquid into a labelled test tube. Rinse the residue with 10 mL 25% CH_3COOH twice. Add the supernatant rinses to the test tube and analyze solution.
5. Residue –resistive minerals	Rinse residue with MilliQ water and oven dry at 60°C. Grind to ≤ 200 µm. Fuse with 12:22 Norrish flux (lithium metaborate/lithium tetraborate). Heat in muffle furnace for 1050°C for 30 min. Dissolve fusion beads in 100 mL 10% HCl and analyze.

In the present study, REE contents including lanthanide elements and Y in regolith samples were normalized (i.e., REE_N) using the chondrite reference value by Taylor and McLennan [24]. The REE distribution patterns were estimated by LREE/HREE and Ce/Ce* ratios. The LREE/HREE values are non-chondrite normalized, and LREE refer to La–Sm while HREE refer to Eu–Lu and including Y. The Ce anomaly (Ce/Ce*) was calculated by $\{2{*}Ce_N/ [La_N + Pr_N]\}$.

3. Results

3.1. Geological Setting

3.1.1. Regional Geology

The studied REE occurrences are located in the Albany-Fraser Orogen (AFO) wrapping around and extending for over 1200 km along the southern and southeastern margins of the Yilgarn Craton. It is dominated by Paleoproterozoic and Mesoproterozoic rocks that formed along the margin of the Archean Yilgarn Craton, due to continuous reworking of the margin [25,26]. Fragments of Archean crust, remnants of the Yilgarn Craton, are preserved within the Proterozoic crust that forms the bulk of the orogen.

The AFO is subdivided into two main tectonic domains: the Archean to Paleoproterozoic Northern Foreland (Figure 1), and a younger, Paleoproterozoic to Mesoproterozoic amalgamation basement component of the Kepa Kurl Booya Province [7]. The Kepa Kurl Booya Province is further divided into the fault-bound tectonic units of the Biranup Zone, the Fraser Zone, and the Nornalup Zone [7; 25, 27].

Most known REE prospects are related to the Biranup and Nornalup Zones with several occurrences recorded in the Northern Foreland. The REE mineralization is hosted by Archean to Mesoproterozoic felsic gneisses and Mesoproterozoic granitoids with minor enclaves of metamorphosed mafic rocks.

1. *Archean (c. 2800-2660 Ma) tonalitic to monzogranitic Munglinup Gneiss of the Northern Foreland.* The granulite-facies Munglinup Gneiss is a higher metamorphic grade component of the Northern Foreland, exhumed from deeper crust levels [7]. The Munglinup Gneiss comprises amphibolite to granulite grade orthogneisses, interlayered with lenses of metamorphosed mafic rocks, with minor banded chert, amphibolitic schist and metamorphosed ultramafic rocks, which are interpreted as remnants of Archean greenstone sequences [7]. The most abundant phase in the Munglinup Gneiss is a leucocratic, mostly homogeneous, banded tonalitic to monzogranitic gneiss (Figure 2a) of the weakly peraluminous composition.
2. *Paleoproterozoic (c. 1690–1660 Ma) metagranitic Dalyup and Coramup Gneisses of the Biranup Zone.* The Dalyup Gneiss is the main component of the Biranup Zone; it is composed of heterogeneous, usually intensely deformed and metamorphosed up to granulite facies granitic rocks, and less abundant mafic rocks. Rock types include granodioritic, monzogranitic, and syenogranitic gneisses, orthopyroxene-bearing granitic gneiss, quartz–magnetite gneiss, mafic gneiss, and

 doi:10.20944/preprints202408.1070.v1

amphibolite [28–30]. Unlike the Dalyup Gneiss, the Coramup Gneiss contains both orthogneisses and paragneisses. Rock types include granitic to granodioritic gneiss, tonalitic gneiss, lenses and boudins of metamorphosed mafic rocks, quartz-rich psammite, and minor migmatitic metapelite [31,32]. At Newmont (Salazar project) especially in the western part, REE mineralization also develops over elongated para-amphibolite bodies of plagioclase-hornblende-biotite composition although REEs seem to have originated from contact zones with surrounding granitic gneisses [18].

3. *Mesoproterozoic (c. 1330-1280 Ma) metamorphosed monzogranites and granodiorites of the Recherche Supersuite* dominate the Nornalup Zone, masking much of the original Paleoproterozoic (c. 1800-1650 Ma) basement. The granitoids comprise foliated metagranites or gneisses with syenogranitic, monzogranitic and granodioritic compositions. Most of the Gora Hill suite granitoids are related to the A-type granites (Figure 2b). Weakly peraluminous granites of the Southern Hills suite are assigned to the I-, S- or M-type granites. Most of these rocks appear to be mingled with a mafic component, generally present as enclaves of various sizes.
4. *Mesoproterozoic (c. 1140 Ma) granites, monzogranites and syenogranites of the Esperance Supersuite.* These granitoids represent the late-stage magmatism of the Albany– Fraser Orogeny, at c. 1140 Ma [7,29,33]. Rocks of the Esperance Supersuite are relatively undeformed and of low metamorphic grade [34]. The A-type, weakly peraluminous to metaluminous monzogranites of the Booanya Suite assigned by chemical composition (Figure 2) within the Esperance Supersuite occur within 90 km-wide, northeasterly trending, generally magnetic belt in the eastern Nornalup Zone [26]. Weakly peraluminous granites of the Truslove suite are assigned to the I-, S- or M-type granites.

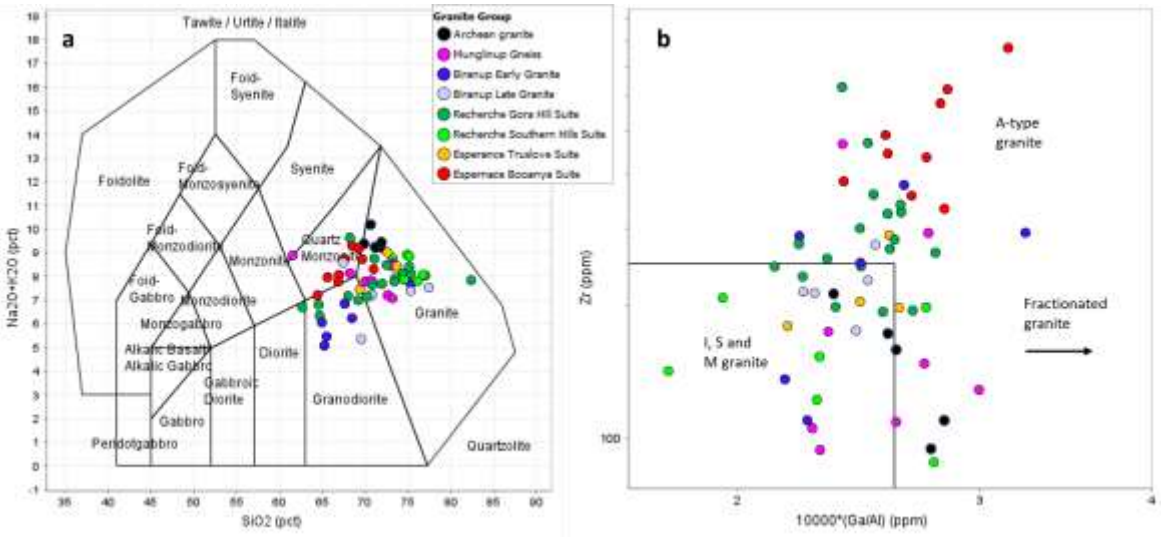

Figure 2. Chemical classification diagrams showing types of major granitoid felsic gneiss types in the Esperance region: a – TAS plutonic classification diagram [35]; b – A- and I-S-M-type granite differentiation diagram [36]. Chemical data source: [26].

Archean granites occurring as relic fragments within the Biranup Zone, show the lowest, 115-229 ppm TREO content compared to other granite groups of the Esperance region (Table 3). Most Proterozoic felsic gneisses and granitoids there show relatively high, 226-323 ppm TREO abundances. The ferroan A-type granites of the Booanya Suite in the youngest Esperance Supersuite are strongly enriched in REEs (especially LREEs), Th, U and HFSE compared to all other granite groups of the AFO [26]. The role of hydrothermal alteration in REE pre-concentration is unknown although REE mineralization at Newmont may be partly sourced from the numerous shear zones [15]. The protolith granitoids, except the Truslove and Southern Hills suites have a relatively high P_2O_5 (>0.08%) content, likely leading to the precipitation of REEs from groundwater as secondary phosphates in the weathering environment [12].

 doi:10.20944/preprints202408.1070.v1

Table 3. Concentrations of REE in major protolith granitoids of the Esperance region. Data source: [26].

Tectonic Zone	Geological Unit	Suite	Age (Ma)	Sample Number	TREO (ppm)		
					Minimum	Maximum	Average
Biranup Zone	Archean granite		2634-2684	5	115	229	155
	Proterozoic granite		1660-1800	10	104	330	230
Northern Foreland	Munglinup Gneiss		2630-2660	8	29	584	246
Nornalup Zone	Recherche Supersuite	Gora Hill	1316-1322	18	166	527	323
		Southern Hills	1300-1320	6	183	258	226
	Esperance Supersuite	Booanya	1172	9	725	1090	880
		Truslove	1162-1196	4	117	383	251

3.1.2. Geomorphology and Regolith

The region is part of the ancient, partly eroded Great Plateau of Western Australia — a vast terrain of gently undulating and subdued relief [37–39]. Palaeogeographical reconstructions indicate that southern parts of Western Australia have been exposed to subaerial conditions since at least the Paleozoic [40–43]. The AFO has a step-like topography; an incipient etchplain with complete lateritic weathering profiles retained in the broad upland divides on the Yilgarn plateau to the north.

In the Esperance region, a broad, southeast trending, low-angle slope descends from the 400 m Yilgarn surface to a degraded paleo-escarpment at 150–200 m AMSL interpreted as a Late Eocene sea-cliff [44,45]. In plan view, the broad slope follows the margin of the Eucla Basin. The top of the Upper Eocene Pallinup Formation sedimentary succession is presently at an elevation of 50–100 m, suggesting a further 80–130 m of tilting in this area, presumably due to greater Eucla Basin subsidence [39].

The mineralized in REE area is mainly related to the partially stripped etchplain (Figure 3) with weathering profiles truncated to the clay saprolite or saprolite with about 20-30 m of regolith retained. Four major deposits are located along a major drainage divide known as the “Jarrahwood Axis” [46]. The southern parts of the region hosting Cascade and Condingup REE prospects are more eroded with only 10-20 m profiles retained for 10-40% of the landscape [47].

 doi:10.20944/preprints202408.1070.v1

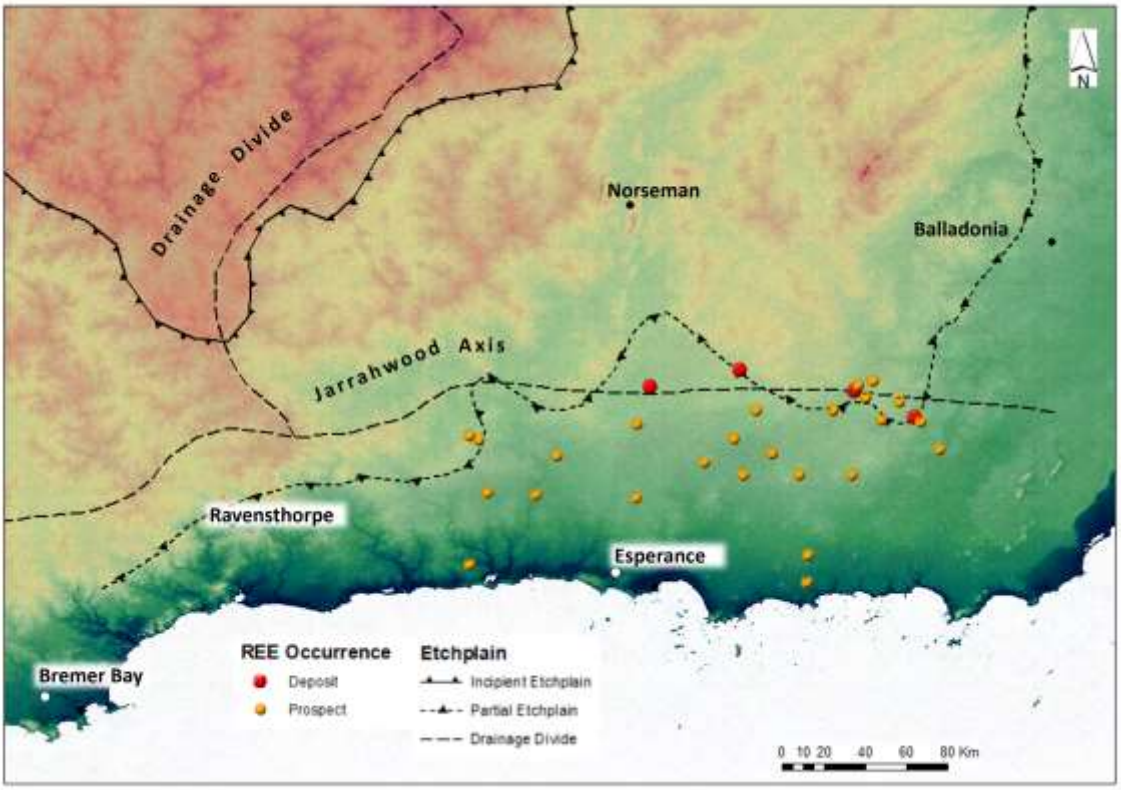

Figure 3. Digital elevation model of the Albany-Fraser Orogen showing distribution of etched surfaces and REE occurrences. Modified after [48–50].

Transported cover is widespread with only isolated small bedrock outcrops encountered. The top part of overburden is dominated by a thin, generally 1-3 m thick, veneer of eolian Quaternary sands. The sand dune formations increase in thickness to 20 m near the shoreline [51]. The sand is commonly calcareous with the subsurface calcrete horizon, locally (e.g., in the Newmont area) 1-3 m thick. Sands are commonly underlain by Eocene sediments of the Plantagenet Group, divided into the Pallinup and Werrilup Formations. These formations vary from non-existent to up to over 60 m deep in paleochannels. Within the Circle Valley deposit, the Eocene, interpreted as lacustrine to shallow marine sediments are up to 20 m, averaging at 10 m [11]. The Pallinup Formation is observed as loosely consolidated grey clays and quartz sands. The underlain Werrilup Formation often presents with an organic-rich basal layer, with rare horizons of clean coarse sand defining the unconformable contact with the underlying weathered basement. At Cowalinya, the Eocene sandy clays, brown sands and loams are commonly silcretised near the base, with ferricrete and colluvium locally present [8]. Relatively deep, up to >60 m thick Cenozoic paleochannels are common in the area; they contain sand, silt and clayey sediments, with overlying carbonaceous clays and lignite in deeper channels [20].

Residual regolith over felsic gneisses and granitoids is topped by upper saprolite although mottled and pallid clay zones are common at some locations [20]. The clay zone and upper saprolite is dominated by quartz and kaolinite [52]. The upper saprolite is commonly grey in color and up to 20 m thick (averaging 10-15 m). The thickness of this upper, clay-rich zone varies widely at some locations depending on bedrock lithology, structural setting and paleogeomorphology (Figure 4). The lower saprolite is grey-green and mainly composed of quartz with minor kaolinite, feldspars, hydromuscovite, iron oxyhydroxides and vermiculite after biotite. The unit is commonly 10-20 m thick. The proportion of clay in the composition of this zone is not reported although can be indirectly estimated based on results of metallurgical beneficiation tests. Thus, an amount of silt (<25 μm fraction) for the lower part of the Cowalinya deposit ranges from 20.8 to 37.8 wt.% (averaging at 31.7

 doi:10.20944/preprints202408.1070.v1

wt.%; [53]. At the Newmont prospect, the silt (<38 μm) fraction comprises 20-49 wt.% with average of 29.5 wt.% [18]. This data suggests relatively low, less than 15 wt.% input of clay (<3 μm) fraction into the composition of the lower saprolite. The saprock is generally thin (1 to 5 m thick). The base of weathering broadly undulates depending on lithology and structural characteristics of protolith.

3.2. Regolith REE Mineralization

Supergene REE mineralization developed within the residual regolith over all major Archean and Proterozoic felsic lithologies across the Esperance region. It occurs as laterally extensive or patchy, subhorizontal, commonly undulating with bedrock topography layers in the lower half of the weathered zone. A single enriched horizon occupying the lower saprolite and saprock is the most common distribution pattern (Figure 4). At some locations (e.g., the Newmont and Prop prospects), two stacked, partially abutting, enriched layers have been delineated. At Newmont, the upper enrichment zone is commonly close to the contact between the upper and lower saprolite, and the lower mineralization "blanket" is in the lower half of the lower saprolite zone (Figure 5). A positive Ce anomaly is common in the upper regolith although its distribution pattern is inconsistent from hole to hole. Heavy REEs generally concentrate with depth down the profile relative to LREEs, although inconsistent, seesaw patterns are also common.

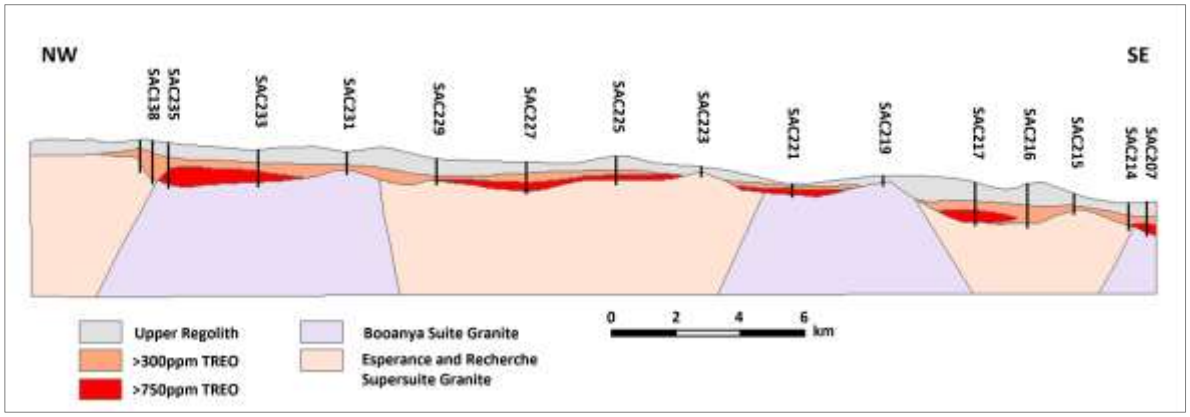

Figure 4. Regolith cross-section showing REE distribution, Splinter Rock deposit, looking NE, x20 vertical exaggeration. Modified after [54].

 doi:10.20944/preprints202408.1070.v1

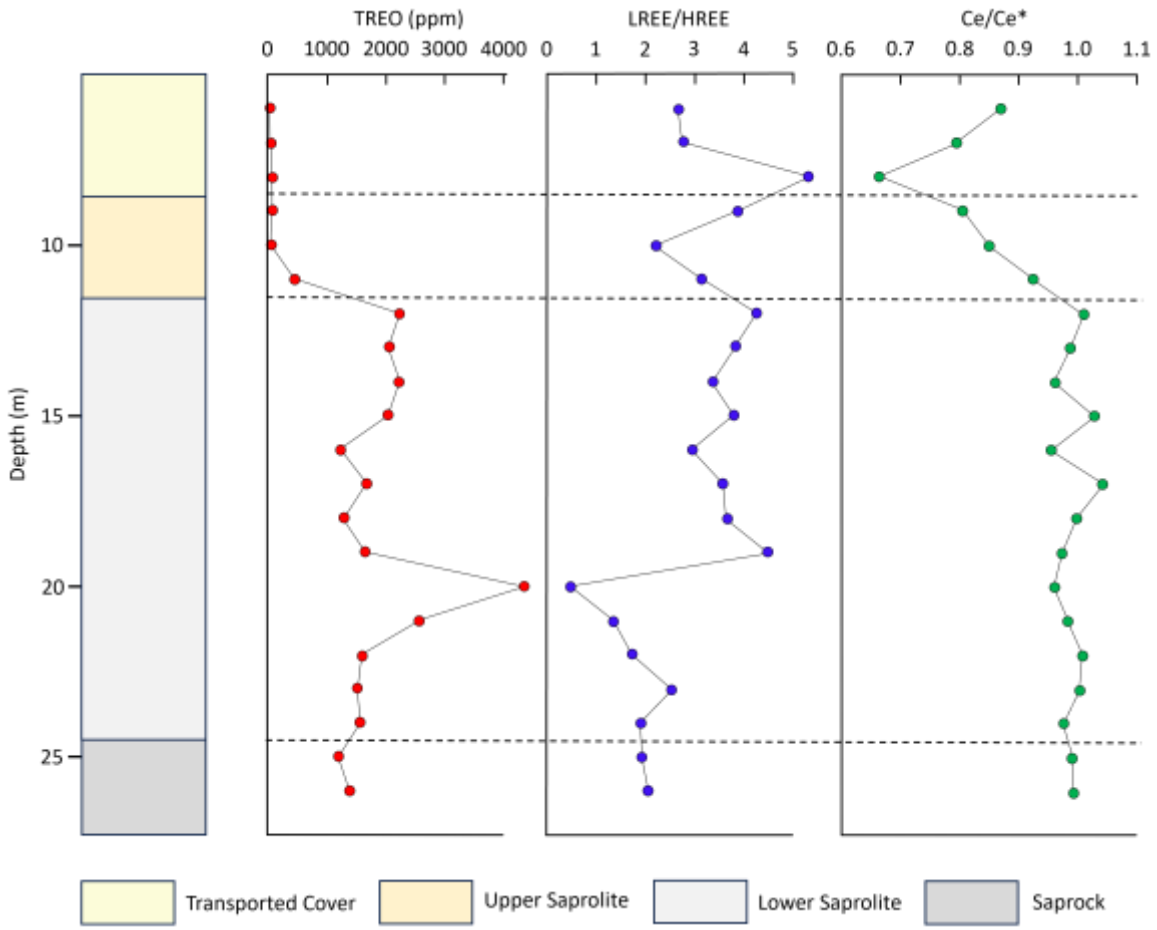

Figure 5. REE distribution through the weathering profile over granodiorite in SAC365 at the Newmont prospect, Salazar project: (a) TREO vertical distribution; (b) Ce/Ce* ratio distribution; (c) LREE/HREE distribution, Data source [55].

At Cowalinya North, three stacked, partially abutting horizons have been recorded (Figure 6) [8]. The top of mineralization is up to 25 m deep and averages at 13 m below the surface. The three mineralized layers occur in the upper, middle, and lower saprolite respectively. The lower layer is the most pronounced, with an average thickness of 6.1 m and TREO content of 522 ppm. The top layer is 3.8 m thick (235 ppm TREO) and the mid-saprolite horizon is 4.7 m thick (465 ppm TREO). The maximum vertical range of the mineralization is up to 63 m.

 doi:10.20944/preprints202408.1070.v1

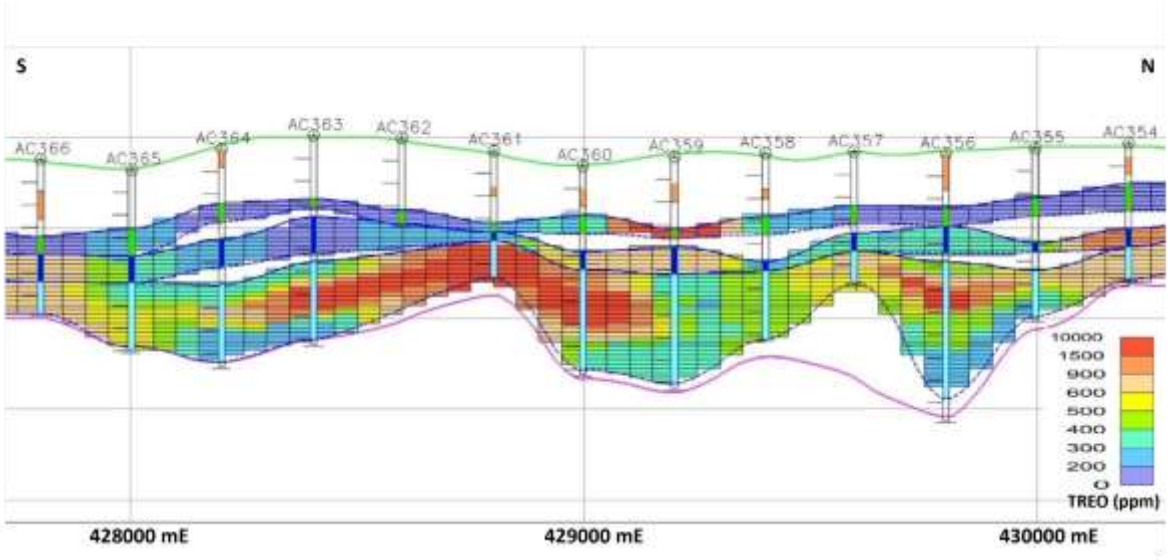

Figure 6. REE distribution in the regolith at the Cowalinya deposit, based on the block model. Section 6357800 mN, looking west. Purple line represents base of weathering. Modified after [8].

In all the other major resources reported, REEs are concentrated within a single enriched horizon occupying the lower saprolite and saprock zones. Average TREO values generally range 800-1300 ppm from site to site reaching a maximum of 6400 and 7475 ppm at the Centre and Circle Valley deposits respectively [56,57], with several drilling intercepts of up to 1.0-2.9% TREO recorded at the Mia prospect in the Mt Ridley project [58].

The upper parts of residual regolith above the mineralization are low in REEs indicating a chemogenic-type enrichment pattern, with REE depletion from the top and accumulation in the lower parts of the weathering profile.

The mineralization is strongly enriched in LREEs, with LREE/HREE up to 31.7 (averaging 9.0) based on data from 13 drill holes at Newmont, Circle Valley, Centre and Matilda South [55–57,59,60]. The $(La/Yb)_N$ ratio, commonly used as an LREE/HREE index [61], broadly ranges from 1 to 115 (averaging 37). The LREE/HREE ratio generally reduces downward indicating HREE fractionation due to their preferential remobilization from the top and accumulation in the lower part of the weathering profile. It should be noted that the vertical LREE/HREE distribution pattern is inconsistent from site to site and irregular seesaw patterns are not uncommon.

Individual REE distribution patterns through a weathering profile in the form of chondrite-normalized spider plots using normalization values from Taylor and McLennan [24] are displayed in Figure 7.

The REE-leached zone above mineralization is enriched in Ce with a negative Ce/Ce* anomaly common within the REE accumulation zone below. Cerium usually separates from the rest of REEs during weathering due to the oxidation of Ce^{3+} to immobile Ce^{4+} and its subsequent fixation as secondary phases in the upper part of weathering crust [12,62–66].

Weathered granitoids at Newmont and Circle Valley display relatively flat patterns with the Newmont granodiorites demonstrating strong negative Eu anomalies through the whole profile. REE distributions from the Centre and Matilda South prospects show relatively steep patterns indicating relative enrichment in LREEs. Apart from the Ce and Eu anomalies, the element distribution patterns remain similar through the weathering profile with lower REE grades observed for the upper REE-leached zone.

 doi:10.20944/preprints202408.1070.v1

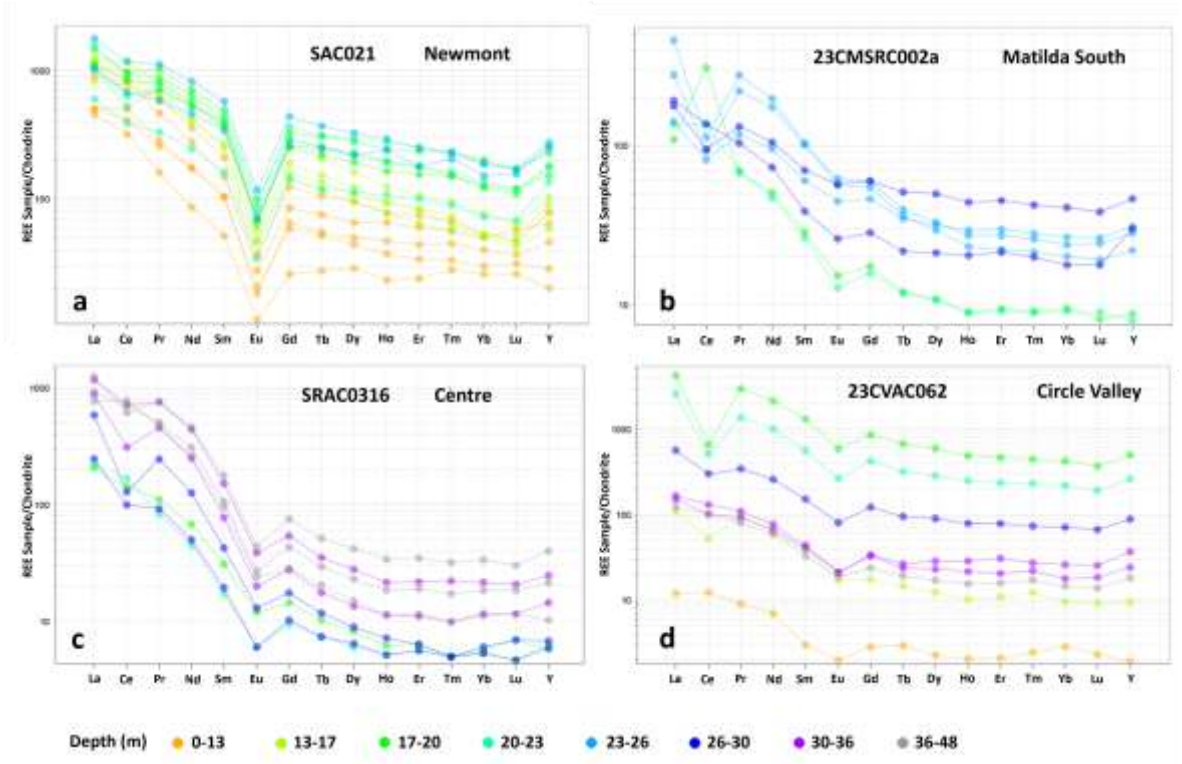

Figure 7. Spider diagrams showing distribution of REE through the weathering profile and bedrock: a - Newmont deposit, drill hole SAC021 [55]; b - Matilda South prospect, drill hole 23CMSRC002a [59]; c - Centre prospect, drill hole SRAC0316 [56]; d - Circle Valley deposit, drill hole 23CVAC062 [57].

3.3. Rare Earth Element Speciation

Open-file information on REE mineralogy in protore bedrock granitoids of the Esperance region is limited to a few studies on the Newmont [15,67,68] and Circle Valley prospects [11]. At Newmont, REEs in the protore granites of the Biranup Complex are mainly hosted by monazite with minor to rare zircon, xenotime, allanite, apatite, titanite, synchysite and cerite (Figure 8). Monazite is of the Ce-La-Nd-Pr composition in decreasing element concentration order. It mainly occurs as euhedral to subrounded grains ranging from 40 to 500 μm in size. Very fine-grained, less than 10 μm, closely associated with biotite, monazite crystals were also recorded [68]. At Circle Valley, mineralization developed over granitic gneisses of the Biranup Zone. The REEs there occur as apatite, monazite, xenotime and zircon [11].

Garnet is another potential REE carrier in the garnet-bearing varieties of granitic gneisses in the Northern Foreland and the Biranup Zone. Garnets of various compositions were reported as minor REE hosts in bedrock at the Longnan IAC-type REE deposit in China [12] and at several deposits in the southeastern United States [69], although their contribution to regolith mineralization has been considered insignificant. No further data on REE content in garnets and their weathering products in the Esperance region is available to date; this warrants further investigation.

In saprolite at Newmont and Cowalinya, REEs are mostly hosted by residual monazite and xenotime with minor contributions from secondary monazite, rhabdophane and churchite/britholite phases. Secondary monazite and rhabdophane commonly occur as less than 2 μm anhedral grains disseminated throughout the kaolinite matrix [15]. The supergene Y-churchite or Y-britholite form rims around zircon grains.

 doi:10.20944/preprints202408.1070.v1

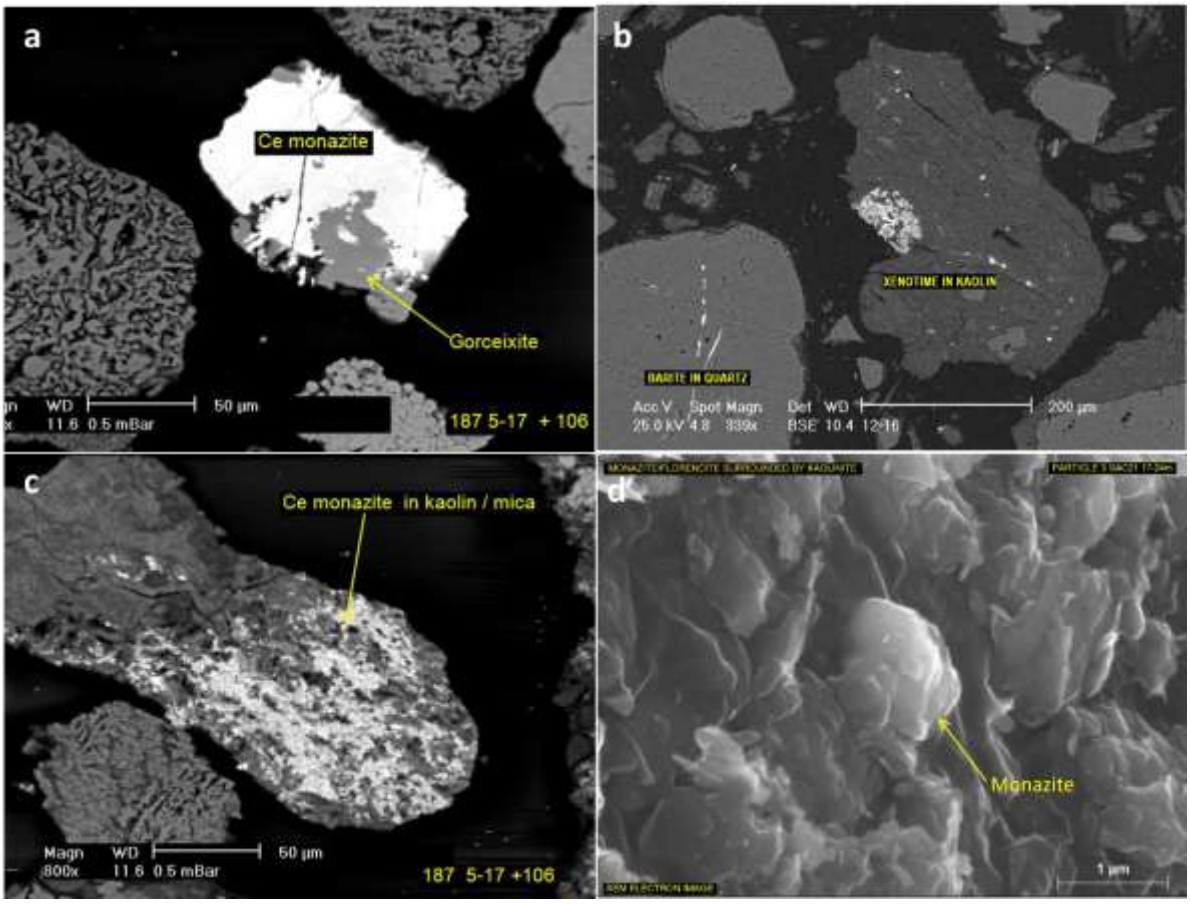

Figure 8. Back-scattered electron SEM images of REE minerals: (a) Residual monazite in close intergrowth with gorceixite [67]; (b) Xenotime in kaolinite matrix [70]; (c) (?)Secondary monazite in kaolinite/muscovite matrix [67]; (d) Secondary monazite in kaolinite matrix [71].

Contribution of non-mineral, ion-adsorbed form of REEs were assessed at several prospects using metallurgical leach tests. An amount of ion-adsorbed REEs recovered by 0.2 mol/L ammonium sulfate at pH 4-5 was negligible, less than 2% for the prospects reported [13–15]. Further leaching tests by a hydrochloric acid at low pH were more successful, showing significant, 49-68% extraction rate of TREEs and Permanent Magnet REEs (PMREE = Pr+Nd+Tb+Dy) at 20°C (Table 4). These results indicate a prevalence of mineral and Fe-Mn oxide-bound colloidal forms of REEs in the enrichment zone.

Table 4. Results of metallurgical leach tests of mineralized regolith by a hydrochloric acid.

Project	Deposit/Prospect	HCl (g/L)	Temperature (°C)	Duration (h)	Recovery (%)	REE Suite	Reference
Cowalinya	Cowalinya South	100	20	24	27	TREE	[14]
Cowalinya	Cowalinya South	25	30	24	71	TREE	[14]
Mount Ridley	*	25	20	24	57	TREE	[16]
Splinter Rock	Centre	25	20	6	49	PMREE**	[17]
Splinter Rock	Prop	25	20	6	68	PMREE	[17]
Salazar	Newmont	25	20	8	68	PMREE	[18]
Salazar	Newmont	100	20	8	78	PMREE	[18]

 doi:10.20944/preprints202408.1070.v1

* - Average for 6 composite samples from Mia, Vincent, Winston and Jody prospects. ** - PMREE - Permanent Magnet REEs: Pr+Nd+Tb+Dy.

More detailed information on REE speciation can be obtained using a sequential extraction method [72–77]. Fifteen downhole samples collected from two drill holes at Newmont and Splinter were studied using the technique described in Section 2 [15]. The samples are from weathering profiles over the garnet-bearing granite gneiss of the Biranup Zone (SAC021) and the granite of the Recherche Supersuite (SAC059) Most of the REEs are hosted by mineral forms (Table 5, over 92% TREE) with minor crystalline Fe oxyhydroxides (0.2-7.1%) and exchangeable fractions (up to 4.8%). Adsorbed and amorphous Fe oxyhydroxide fractions comprise less than 1% of TREE speciation, with many results on the amorphous Fe extraction for individual REEs below the detection limit.

Table 5. TREE content and relative REE speciation through weathering profile over granitoids at the Newmont (SAC021) and Splinter (SAC059) prospects: Drill hole SAC021 - garnet-bearing granite gneiss of the Biranup Zone; Drill hole SAC059 - granite of the Recherche Supersuite. Modified after [15].

Drill Hole	Depth Range (m)	TREE (ppm)	Relative TREE Proportion by Fraction (%)				
			Water-soluble and ion adsorbed	Adsorbed and carbonate bound	Amorphous Fe oxyhydroxide bound	Crystalline Fe oxyhydroxide bound	Residual mineral forms
SAC021	8-10	713	0.00	0.07	0.04	0.75	99.14
	10-14	1134	0.08	0.05	0.01	1.11	98.74
	14-17	1683	0.64	0.17	0.01	4.55	94.63
	17-20	2474	0.50	0.37	0.03	7.09	92.01
	20-24	2398	0.33	0.28	0.03	3.92	95.44
	24-26	2717	4.79	0.36	0.13	1.55	93.17
SAC059	12-15	271	0.29	0.02	0.00	0.17	99.52
	15-17	401	0.12	0.03	0.01	0.88	98.96
	17-21	400	0.15	0.04	0.00	1.43	98.38
	21-26	1704	0.12	0.03	0.00	1.92	97.92
	26-33	2181	0.39	0.08	0.01	3.36	96.16
	33-37	708	1.51	0.09	0.02	1.85	96.53

4. Discussion

4.1. Factors Controlling Regolith-Hosted REE Mineralization

The formation of regolith-hosted REE deposits is generally an interplay between endogenic and weathering processes. Ion-adsorption clay deposits, the only exploitable type of regolith clay-hosted REE deposits to date, are formed by the weathering of felsic magmatic rocks with elevated REE content. The most favorable parent rocks are evolved or/and hydrothermally altered granitoids and felsic volcanics of HREE affinity. The critical requirement is the prevalence of primary REE minerals that are easily susceptible to weathering, e.g., REE fluorocarbonates, REE-bearing fluorite, apatite, titanite, and allanite [12,78–80]. A protolith with low P, Fe and Mn content is also an important factor ensuring a deficit of cations that could strongly bind REEs as secondary minerals or in colloidal form in the weathering environment [12].

In terms of weathering processes, climate and geomorphological setting were considered to be the key controls for formation of IAC-type mineralization [12,81–84]. These parameters facilitate the dynamic balance between active chemical weathering and denudation rate. A subtropical humid climate with a high rainfall input (e.g., 1500–2000 mm per annum in Southern China] promotes active chemical weathering to form a thick zone of kaolinite and halloysite clays [61]. Geomorphology also

 doi:10.20944/preprints202408.1070.v1

plays an active role as thicker weathering crusts and IAC orebodies are formed on hill tops and upper slopes due to the active hydrogeological regime and lower intensity of fluvial incision and erosion. A low to moderate denudation rate is required to maintain an active weathering process in advance of continuous physical removal of constituents and subsequently preserve the forming mineralization zone [12,61].

Climatic conditions and geomorphology also greatly affect Eh-pH conditions, input of organic substances and hydrogeochemical regimes favorable for supergene dissolution of primary REE-bearing minerals, mobilization of REEs in the upper unsaturated zone, their downward migration and concentration in the ion-adsorbed form in the clay zone [12,72]. Continuous cycling of such a dynamic system gradually enriches the weathering crusts with REEs to form ore grade accumulations. In these processes, REEs may fractionate to a certain degree due to higher mobility of HREEs in oxidizing acid environments. The most favorable hydrogeochemical regime includes near-surface acidic groundwaters and a gradual increase in pH to neutral in the clay zone encouraging adsorption of REEs onto kaolinite particles.

4.2. Potential Mineralization Controls in the Esperance Region

REE mineralization in the Esperance region demonstrates a number of characteristics similar to that observed for IAC-type deposits. The mineralization occurs as continuous flat-lying enrichment "blankets" within the saprolite. The enriched horizon is coupled with the depletion zone above indicating chemogenic type enrichment characteristic of many other regolith mineral systems (e.g., Ni, Cu, Zn and Au) [85,86]. Furthermore, fractionation of HREEs with a gradual downward increase in HREE/LREE ratio and the presence of new-formed REE minerals in the lower part of the weathering profile, indicate re-mobilization, downward transport and accumulation of HREEs as the supergene enrichment horizon. Mineralization was also contributed by the residual REE accumulation process due to bulk rock volume and mass removal during the weathering.

However, there are important differences between the local REE occurrences and the IAC deposits. In the Esperance region, the REE enrichment zone is positioned deeper in the weathering profile, in the lower part of saprolite and saprock, and consequently has relatively low clay content. Most importantly, the known-to-date regolith REE occurrences in the region lack an ion-adsorbed REE component with the REEs dominated by residual and secondary mineral forms. Processing this type of ore requires the use of acid leaching for REE recovery, resulting in higher costs which affects the economic viability of projects.

This lack of ionically-adsorbed REEs can be partly due to the specific characteristics of the protolith. Although REEs in parent rocks are mainly hosted by resistant to weathering monazite, zircon and xenotime, there is evidence of secondary phosphate minerals in the mineralized zone. As most protoliths have a relatively high phosphorus content, its dissolution and migration in groundwater could prevent physical adsorption onto clay particles by fixation of the REE-ions as secondary phosphates.

Parent rock composition and REE speciation definitely contribute to regolith mineralization, but it is hard to explain similar REE distribution patterns and the uniform lack of ion-adsorbed REE component across this large region by these primary factors alone, considering the existing differences in composition, metamorphic grade and age over a variety of protore granitoids and felsic gneisses across the region. This emphasizes the important role of weathering processes in the behavior of REEs in the regolith environment possibly overprinting differences between the primary sources. Climate history and related groundwater hydrochemistry are thought to be the main drivers of the intense REE mobilization and redistribution in the region, resulting in enrichment near the weathering base and non-adsorbed REE speciation in the mineralized zone.

Geomorphology also contributed to the resulting supergene mineralization. The planation of the relief led to slowing down erosion and preservation the existing mineralization. The location of all major deposits along the "Jarrahwood Axis" major drainage divide likely reflects a more active hydrogeological regime on the hill tops, which contributed to more intense weathering and supergene REE enrichment.

 doi:10.20944/preprints202408.1070.v1

4.3. Climate Evolution and Hydrogeochemistry

The Esperance region has a long and complex weathering history. The paleoclimate and weathering evolution of the region have been summarized by Anand and Butt [49] and Gonzalez-Alvarez et al. [87] as:

1. Glacial erosion during the Early Permian followed by Palaeozoic and Mesozoic weathering that eroded many of the pre-existing geomorphologic features;
2. Humid and sub-tropical conditions in the Late Cretaceous that promoted intense chemical weathering;
3. Sea-level changes in the Late Cretaceous–Mid Eocene resulting in erosion and active sedimentary processes that reshaped the landscape;
4. Intense weathering under humid tropical-sub tropical conditions during the Paleocene and Eocene; and
5. Climate conditions changed to semi-arid and arid in the Neogene and Quaternary.

These shifts had a large impact on the sedimentation and weathering environments, resulting in increased groundwater salinity and a slowdown in erosion rates [47,88–90].

In southwestern Australia, low relief landforms cover about 95% of the landscape [48]. During the Late Mesozoic-Early Cenozoic, intense lateritic chemical weathering developed widely throughout the region under humid sub-tropical to tropical climate [49]. The weathering profiles were preserved due to sea-level regression during the Oligocene: water tables dropped due to increased aridity, resulting in induration of the weathering profiles. Subsequent climatic changes produced varying degrees of erosion, truncating the lateritic profiles, and distributing the debris as sedimentary packages in the surrounding areas. This process aided in flattening the landscape by filling low areas. Finkl [48] interpreted the low relief landforms in the southern Western Australia as a series of plains, where lower plains were successively stripped from higher plains to produce a step-like topography (etchplains).

The Esperance region currently experiences a cold semi-arid climate except for the southernmost strip along the coast which has a Mediterranean climate. Cold semi-arid climate features warm to hot dry summers and relatively cold winters. The annual rainfall is highest in the southwest and decreases north and eastwards averaging at 300-500 mm in the study area.

Climate aridification since the Oligocene led to the formation of acidic (pH <4) and saline (total dissolved solids (TDS) over 20,000 mg/L) groundwaters on a regional scale [50]. The region is considered to be part of one of the largest provinces of naturally occurring acidic waters in the world [91] which extends from Western Australia [92–95] through South Australia [96–98] to Victoria [99,100].

Acidic groundwaters become progressively more common further from the coast towards the drier internally drained regions [50]. The number of acidic groundwater wells significantly increase from the coastal (< 10%) to the drier internal areas (> 40%, Figure 9). The area dominated by acidic groundwaters is likely even more widespread as the data from remote inland areas are limited.

Preprints.org (www.preprints.org) | NOT PEER-REVIEWED | Posted: 14 August 2024 doi:10.20944/preprints202408.1070.v1

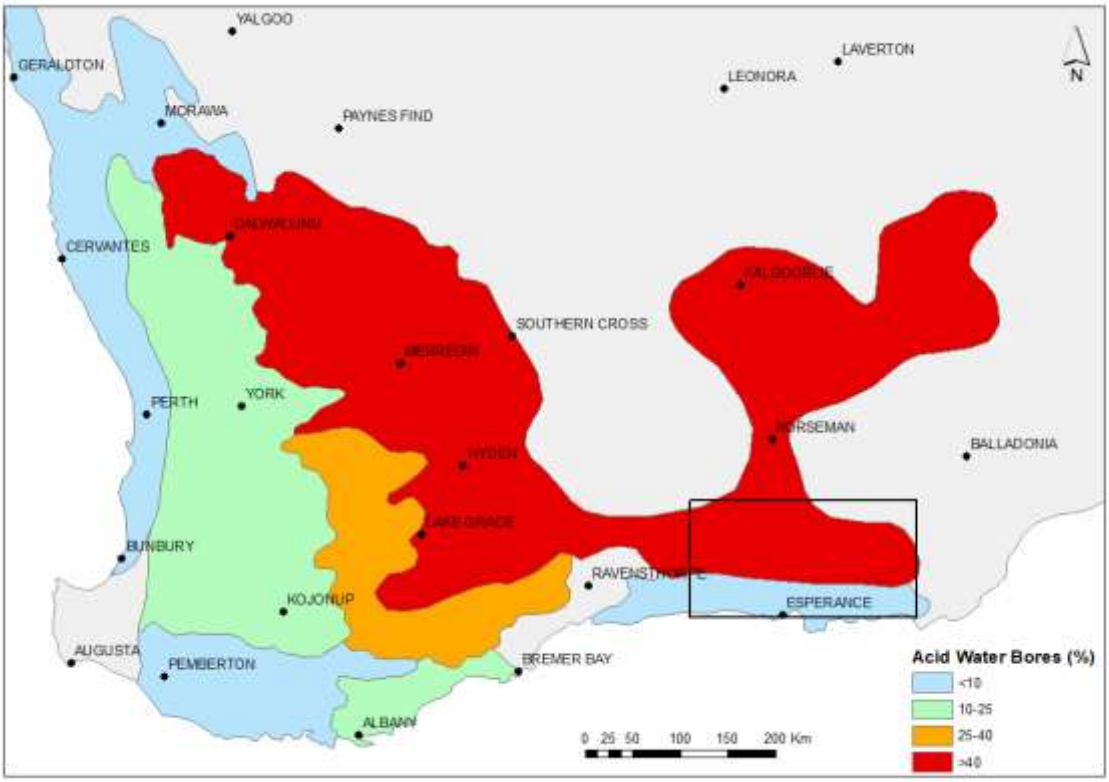

Figure 9. Percentage of acidic groundwater wells across south-western Australia [49,50].

Acidic saline groundwaters are mostly related to the areas of Eucalyptus mallee woodlands developed on alkaline calcareous soils. Vertical pH distribution in these areas looks paradoxical at first sight as the upper 1 m of the subsurface unsaturated zone has a pH around 8 while the pH at depths more than 5 m decreases down to <4 (Figure 10) [50,95].

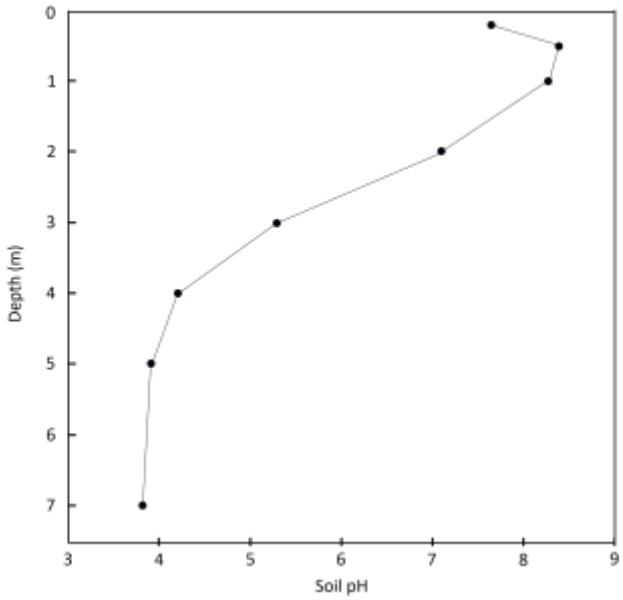

Figure 10. Historic soil data showing average soil pH at different depths at five study sites near Burvill, Salmon Gums area [50,95].

 doi:10.20944/preprints202408.1070.v1

Similar downward pH changes from 6.1 at 3 m depth to 3.1-2.8 below 15 m depth were recorded in the water bore BS109 located in the Newmont prospect area [15]. Analyses of groundwater from 11 of 13 exploration drill holes tested around the Newmont and Splinter prospects returned pH 2.8-3.7 with TDS ranging from 32,400 to 105,400 mg/L indicating strongly acidic, highly saline to hypersaline groundwater compositions [55].

A number of mechanisms have been proposed to explain acidification of groundwater in the arid environment [92–95,101,102]. The biogeochemical theory was first proposed by Gray and Noble [101] and further developed by Lillicrap and George [103], and Lillicrap [50] for the southwest of Australia. It was suggested that acidified profiles at depth can be created through reactions mediated by soil bacteria and fungi found in the tree root zone by iron enrichment of regolith in the unsaturated zone combined with calcification [50]. Calcium for formation of the subsurface pedogenic calcrete horizon is sourced from the deeper profile where the root biota exchanges calcium for hydrogen ions to maintain charge balance. Iron is mobilized from the soil and concentrates lower in the profile (depths >1.5 m). There, the iron is microbially reduced around roots and the alkalinity generated by microbial iron reduction is removed by biogenic calcification processes. The iron moves in solution further down the profile following roots into the oxygenated unsaturated zone matrix where it is oxidized generating acid. The resulting solution acidifies the unsaturated zone matrix. Saline groundwater moving through the matrix becomes acidified due to ion exchange or direct recharge. Geochemical calculations in PHREEQC supported the proposed model obtaining acid solutions with a pH of 3.8 or lower [50].

4.4. REE Mobility in Acid Groundwaters

Dissolution of REEs in groundwaters is known to be strongly controlled by pH, redox conditions, and aqueous and surface complexation reactions [104–109]. Review of data on REE geochemistry in groundwaters by Noack et al. [110] showed that pH provides the key control over dissolved REE abundances of all the bulk solution chemistry parameters. Concentrations of REEs greatly, up to several orders of magnitude, increase with lowering pH down to 3-4 in surface and groundwater [110–112]. Similar trends were observed for waters in the Acid Mine Drainage environment [113–117].

At neutral and basic pH, REEs are effectively scavenged from groundwater via sorption onto Fe-Mn oxyhydroxides and clays or through coprecipitation with carbonates and phosphates by replacing Ca, which has a comparable atomic radius [117].

Data from 13 drill holes at the Newmont and Splinter prospects showed strongly anomalous, from 546 to 3982 ug/L TREE concentrations in acidic (pH 2.9-3.7) groundwaters [55]. In contrast, neutral to slightly alkaline (pH 7.4-8.2] groundwaters from three local drill holes there only showed background, below detection limit REE abundances.

Limited data from the water bore BS109 in the Newmont area (Table 6) showed anomalous, up to 394 ug/L TREE values in acid groundwaters below a water table with the most anomalous concentrations observed for Y, Nd, Dy and La [15].

Table 6. Downhole REE abundances in water bore BS109, the Newmont prospect. Data source [15].

Depth (m)	REE (ppm)											
	pH	La	Ce	Pr	Nd	Sm	Eu	Dy	Ho	Er	Y	TREE
3	6.1	5	bdl	4	5	bdl	2	bdl	bdl	bdl	5	21
15	3.1	15	50	12	75	25	6	25	6	15	165	394
30	2.8	10	25	6	35	10	4	10	2	5	70	177

Note: bdl = Below detection limit.

The data on increased REE solubility in acid groundwaters in the Esperance region are in a good agreement with the downhole hydrogeochemical data from the Kalgoorlie area to the north. The average dissolved REE concentrations in groundwaters at the Argo, Steinway and Wollubar

 doi:10.20944/preprints202408.1070.v1

paleochannel Au prospects south of Kalgoorlie were 518.7, 1204 and 1656.4 ug/L TREE respectively [118].

The hydrogeochemical data are also in line with research data on the stability of REEs in aqueous and acid-water systems. Kim and Osseo-Asare [119] established Eh-pH diagrams for monazite during a hydrometallurgical process, which covered the Nd-, Ce-, and La-PO_4^{3-}-H_2O systems at 25 °C. The diagrams constructed for the poorly and well-crystalline forms of monazite revealed significant differences between their solubilities (Figure 11). For the poorly crystalline monazite, REE^{3+} ions are stable up to pH 6 and solid $REE(PO_4)$ and $REE(OH)_3$ phases appear as pH increases above this level. The corresponding diagram based on the crystalline phosphate showed that the stability fields of the $REE(PO_4)$ solid phases extend to strongly acidic conditions (pH <1). It was concluded that typical relatively crystalline monazite must be of high chemical stability owing to the higher bond energy.

Shuai et al. [120] studied the aqueous equilibrium of bastnaesite in hydrochloric acid leaching systems. The Eh-pH diagrams in the REE-Cl-H_2O system indicate that trivalent REE^{3+} ions leach into solution at pH values below 6 while tetravalent Ce^{4+} remains in solid forms.

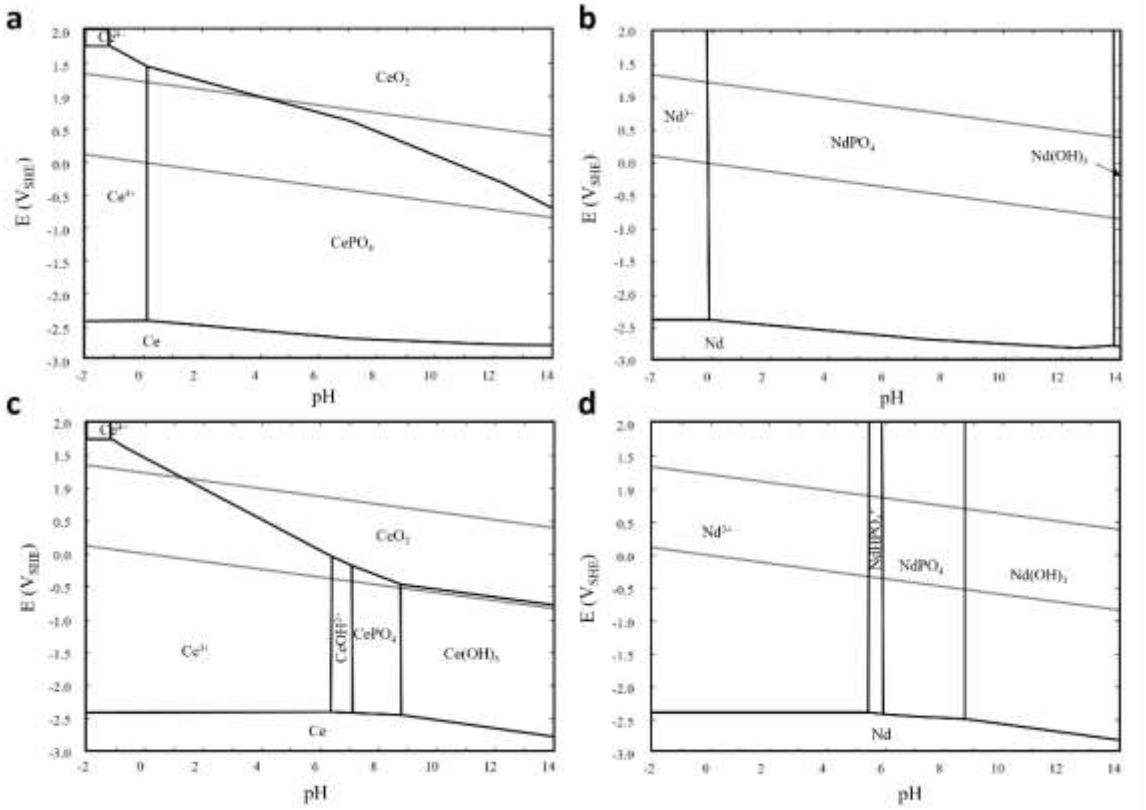

Figure 11. Eh–pH diagrams for the Th–, Nd–, Ce–, La–PO_4–H_2O systems at 25 °C, {PO_4}=10^{-3} M: (a-b) Well-crystalline monazite; (c-d) Poorly crystalline monazite; {Nd} = 10^{-3} M, $\Delta GNdPO_4$ =–423.46 kcal/mol, (c) {Ce} = 10^{-3} M, ΔGC_ePO_4 =– 421.75 kcal/mol, (d) {La} = 10^{-3} M, ΔGL_aPO_4 =–425.78 kcal/mol. Modified after [119].

4.5. An Integrated Genetic Model and Practical Implications

The following integrated model is proposed to summarize the characteristics and explain the genesis of the regolith-hosted REE deposits in the Esperance region. Formation of REE mineralization in the region started in the Cretaceous by active weathering under humid, subtropical conditions continuing to the Mid to Late Cenozoic. Archaean–Proterozoic felsic gneisses and granitoids characterised by elevated REE abundances were modified into deep lateritic weathering crusts. The REEs released from decomposition of rock-forming and accessory primary minerals, migrated downward and were partly adsorbed by kaolinitic clays in the upper parts of the weathering profile.

 doi:10.20944/preprints202408.1070.v1

Resistant to weathering REE minerals remained in situ as residual phases. Part of the migrating in solution or in colloidal form REEs moved deeper into the profile re-precipitating as secondary minerals (e.g., florencite and monazite).

Since the Oligocene, the climate changed to semi-arid to arid conditions leading to the formation of acidic and highly saline groundwaters on a regional scale. These changes intensified the REE dissolution and migration in groundwaters, completely overprinting the pre-existing, possibly the IAC-type REE distribution pattern and mineral speciation. The REEs within the clay zone became unstable under acid conditions and were remobilized and moved downward precipitating at neutral pH in the less oxidizing, clay-deficient environment as colloidal forms bound with Fe and Mn oxyhydroxides, and as secondary mineral forms. The weathering profiles were partly preserved due to the slowing down of erosion and drop in the water table.

The lack of the ion-adsorbed REE component in the areas of acidic groundwaters implies that exploration should focus on more humid areas, less affected by aridification processes, possibly to the southwest. On the Western Australian scale, the northern half of the state north of the "Menzies Line" [88,121], which is characterised by more neutral groundwaters is thought to be more prospective for the IAC type deposits. Active migration of REEs in acid groundwaters may result in transport of significant amounts of REEs along paleochannels where acid conditions remain over large distances as indicated by data from the Argo, Steinway and Wollubar paleochannels in the Kalgoorlie area [118]. The REEs could then precipitate in reducing environments (e.g., in lignite-rich deltaic parts of paleochannels) or at the contact with carbonate rocks due to a rise in pH, forming the Koppammurra style sedimentary deposits.

Conclusions

The regolith-hosted REE mineralization recently discovered in the Esperance region shows many parameters characteristic for the ion-adsorption clay type deposits on a regional scale. The mineralization averaging 800-1200 ppm TREO for major resources was formed by the weathering of Archaean-Proterozoic granite gneisses and granitoids with elevated REE content. It occurs as a single or a series of continuous flat lying enrichment "blankets" within the lower saprolite and saprock. Enrichment in the lower regolith is accompanied by an overlying REE depletion zone, indicating chemogenic type enrichment formed by supergene REE mobilization into groundwater solution, downward transport and accumulation in the lower part of the weathering profile. The mineralization tenor also contains residual REEs accumulated due to bulk rock volume and mass removal during weathering.

Despite some similarities to IAC deposits, there are critical differences preventing assignment of the Esperance occurrences to this class regolith mineralization. Most importantly, the local REE occurrences lack the ion-adsorbed REE component, with the REE dominated by residual and secondary phosphate minerals. This non-adsorbed type REE speciation in the supergene zone can be partly explained by the chemical composition of the protolith, namely a relatively high phosphorus content. Dissolution of P and its migration in groundwater could prevent physical adsorption of REE onto clay particles by fixation the REE-ions as secondary phosphates.

Climate history and related groundwater hydrochemistry are considered to be the key controls affecting the REE behavior in the weathering environment and governing the resulting REE distribution pattern and mineral speciation. Tertiary aridification of climate in southwest Australia heavily overprinted pre-existing REE distribution in the weathering profile. Acidic, highly saline groundwaters intensely leached away any relatively weakly bound, ionically adsorbed and colloidal REE forms, transported them downward and precipitated as secondary phosphates in neutral to alkaline environment at lower Eh near the base of the weathering profile.

Author Contributions: Conceptualization, N.S. and T.C.; methodology, N.S. and T.C.; software, N.S. and T.C.; resources, N.S. and T.C.; data curation, N.S. and T.C.; writing—original draft preparation, N.S.; writing—review and editing, N.S. and T.C. All authors have read and agreed to the published version of the manuscript.

Funding: This research received no external funding.

 doi:10.20944/preprints202408.1070.v1

Data Availability Statement: All data are contained within the article.

Acknowledgments: We are grateful to the ERM Group Pty Ltd. for supporting this work and permission to publish the results. Many thanks to Justin Parker for reviewing the paper and providing valuable comments.

We thank the two anonymous reviewers for their constructive comments, which helped us to improve the quality and clarity of the manuscript, and Filip Costic for the editorial handling of the manuscript.

Conflicts of Interest: The authors declare no conflicts of interest.

References

1. Lusty, P.A.J.; Shaw, R.A.; Gunn, A.G.; Idoine, N.E. UK criticality assessment of technology critical minerals and metals. British Geological Survey Commissioned Report 2021, CR/21/120, 76pp.
2. Department of Industry, Science, Energy and Resources. Critical minerals strategy 2023-2030. Available online: https://www.industry.gov.au/sites/default/files/2023-06/critical-minerals-strategy-2023-2030.pdf (accessed on 19 July 2024).
3. IEA (International Energy Agency). The role of critical minerals in clean energy transitions. Available online: https://www.iea.org/reports/the-role-of-critical-minerals-in-clean-energy-transitions (accessed on 19 July 2024).
4. Liu, S-L.; Fan, H-R.; Liu, X.; Meng, J.; Butcher, A.R.; Yann, L.; Yang, K-F.; Li, X-C. Global rare earth elements projects: New developments and supply chains. *Ore Geol. Rev.* **2023**, *157*, 105428, https://doi.org/10.1016/j.oregeorev.2023.105428
5. Uren, D. Breaking China's near monopoly on rare earths will be easier said than done. The Strategist, 8 November 2022. Available online: https://www.aspistrategist.org.au/breaking-chinas-near-monopoly-on-rare-earths-will-be-easier-said-than-done/ (accessed on 19 July 2024).
6. King, H.M. 2023. REE – Rare Earth Elements and their Uses. https://geology.com/articles/rare-earth-elements/#:~:text=rare%20earth%20metals.-,Uses%20of%20Rare%20Earth%20Elements,fluorescent%20lighting%20and%20much%20more (accessed on 19 July 2024).
7. Spaggiari, C.V.; Bodorkos, S.; Barquero-Molina, M.; Tyler, I.M.; Wingate, M.T.D. Interpreted bedrock geology of the south Yilgarn and central Albany–Fraser Orogen, Western Australia: Geological Survey of Western Australia 2009. Record 2009/10, 84p.
8. Heavy Rare Earths Ltd.; Five-fold increase in mineral resources to 159 Mt @ 870 ppm total rare earth oxides at Cowalinya project in Western Australia; Australian Stock Exchange Announcement, 3 October 2023.
9. West Cobar Metals; Salazar clay-REE resource quadruples to 190 Mt @ 1172 ppm TREO at a 600 ppm cut-off; Australian Stock Exchange Announcement, 9 August 2023.
10. OD6 Metals; Splinter Rock Rare Earth Project Maiden Mineral Resource Estimate 344 Mt @ 1,308 ppm TREO at a 1,000 ppm cut off; Australian Stock Exchange Announcement, 18 July 2023.
11. Meeka Metals; 98 Mt @ 890 ppm TREO – Initial Independent High-Grade Rare Earth Mineral Resource at Circle Valley; Australian Stock Exchange Announcement, 14 June 2023.
12. Sanematsu, K.; Watanabe, Y. Characteristics and genesis of ion-adsorption type deposits. *Rev. Econ. Geol.* **2016**, *18*, 55–79.
13. Rogers, K.A. Esperance Splinter project, exploration licences E63/1415. Annual technical report for the period 12/01/2011 to 11/01/2012. Salazar Gold Pty Ltd. 2012, WAMEX A093149, 59p.
14. Heavy Rare Earths Limited Prospectus. Australian Stock Exchange Announcement, 22 August, 2022.
15. Collins, T. Understanding the geochemistry and mineralogy of regolith hosted REE mineralisation. B.S. Thesis, The University of Western Australia, October 2014.
16. Mount Ridley Mines; Excellent screen beneficiation test results lift REE grades by up to 202% at the Mount Ridley REE Project; Australian Stock Exchange Announcement, 6 July 2023.
17. OD6 Metals; Very high magnet rare earth recoveries achieved at Splinter Rock Project; Australian Stock Exchange Announcement, 3 April 2023.
18. West Cobar Metals; Excellent rare earth metallurgical recoveries achieved at Salazar. Australian Stock Exchange Announcement, 24 July 2023.
19. Crook, D.J.; Brand, N.W. Clay-hosted rare earth element mineralisation in the Esperance district of Western Australia. In Proceedings of the CRITCON, Adelaide, Australia, 22-26 May 2023.
20. Trench, A.; Zhang, L.; Groves, D.I.; Crook, D.; Brand, N.W. Australian critical metal exploration for analogues of Chinese ionic-clay REE deposits. *Geo. Geo.* **2024**, 100293. doi: https://doi.org/10.1016/j.geogeo.2024.100293
21. Shuman, L.M. Fractionation method for soil microelements. Soil Science 1985, 140, 11-22.
22. Hall, G.E.M.; Gauthier, G.; Pelchat, J.-C.; Pelchat, P.; Vaive, J.E. Application of a sequential extraction scheme to ten geological certified reference materials for the determination of 20 elements. *J. Anal. At. Spectrom.* **1996**, *11*, 787- 796.

23. Du, X.; Rate, A.W.; Gee, M.A.M. Particle size fractionation and chemical speciation of REE in a lateritic weathering profile in Western Australia. *Explore* **2012**, *157*, 1-14.
24. Taylor, S.R.; McLennan, S.M. The Continental Crust: Its Composition and Evolution; Blackwell, Oxford, UK, 1985; 312p.
25. Spaggiari, C.V.; Kirkland, C.L.; Pawley, M.J.; Smithies, R.H.; Wingate, M.T.D.; Doyle, M.G.; Blenkinsop, T.G.; Clark, C.; Oorschot, C.W.; Fox, L.J.; Savage, J. The geology of the east Albany–Fraser Orogen — a field guide. Geological Survey of Western Australia, Record 2011/23, 2011, 97p.
26. Smithies, R.H.; Spaggiari, C.V.; Kirkland, C.L. Building the crust of the Albany–Fraser Orogen: constraints from granite geochemistry. Geological Survey of Western Australia, Report 150, 2015, 49p.
27. Myers, J.S. The Fraser Complex: a major layered intrusion in Western Australia, In *Professional papers for 1983*; Geological Survey of Western Australia, Report 14, 1985, pp 57–66.
28. Beeson, J.; Delor, C.P.; Harris, L.B. A structural and metamorphic traverse across the Albany Mobile Belt, Western Australia. *Precambr. Res.* **1988**, *40/41*, 117–136.
29. Nelson, D.R.; Myers, J.S.; Nutman, A.P. Chronology and evolution of the Middle Proterozoic Albany–Fraser Orogen, Western Australia. *Aust. J. Earth Sci.* **1995**, *42*, 481–495.
30. Geological Survey of Western Australia, South Yilgarn Geological Exploration Package: Geological Survey of Western Australia Record 2007/13, 2007.
31. Bodorkos, S.; Clark, D.J. Evolution of a crustal-scale transpressive shear zone in the Albany Fraser Orogen, SW Australia: 1. P–T conditions of Mesoproterozoic metamorphism in the Coramup Gneiss. *J. Metamorph. Geol.* **2004**, *22*, 691–711.
32. Bodorkos, S.; Clark, D.J. Evolution of a crustal-scale transpressive shear zone in the Albany Fraser Orogen, SW Australia: 2. Tectonic history of the Coramup Gneiss and a kinematic framework for Mesoproterozoic collision of the West Australian and Mawson cratons. *J. Metamorph. Geol.* **2004**, *22*, 713–731.
33. Clark, D.J.; Hensen, B.J.; Kinny, P.D. Geochronological constraints for a two-stage history of the Albany–Fraser Orogen, Western Australia. Precambrian Research 2000, 102, 155–183.
34. Myers, J.S. Geology of the Esperance 1:1 000 000 sheet: Geological Survey of Western Australia, 1:1 000 000 Geological Series Explanatory Notes, 1995,10p.
35. Middlemost, E.A.K. Naming Materials in the Magma/Igneous Rock System. *Earth. Sci. Rev.* **1994**, *37*, 215-244. http://dx.doi.org/10.1016/0012-8252(94)90029-9
36. Whalen, J.B.; Currie, K.L.; Chappell, B.W. A-type granites: geochemical characteristics, discrimination and petrogenesis. *Contrib. Mineral. Petrol*. **1987**, *95*, 407–419. https://doi.org/10.1007/BF00402202
37. van de Graaff, W.J.E.; Crowe, R.W.A.; Bunting, J.A.; Jackson, M.J. Relict Early Cainozoic drainages in arid Western Australia. *Z. Geomorphol.* **1977**, *21*, 379–400.
38. *Phanerozoic Earth History of Australia*. Veevers, J.J. Ed.; Clarendon Press, Oxford., UK, 1984.
39. Gammon, P.R.; James, N.P.; Clarke, J.D.A.; Bone, Y. Sedimentology and lithostratigraphy of Upper Eocene sponge-rich sediments, southern Western Australia. *Aust. J. Earth Sci.* **2000**, *47*, 1087–1103. doi: 10.1046/j.1440-0952.2000.00835.x.
40. Daniels, J.L. Palaeogeographic development of Western Australia—Precambrian. *Geological Survey of Western Australia Memoir*, **2**, 1975, pp. 437–450.
41. Playford, P.E.; Cope, R.N.; Cockbain, A.E. Palaeogeographic development of Western Australia—Phanerozoic. Geological Survey of Western Australia Memoir 1975, **2**, 451–460.
42. Butt, C.R.M. Major uranium provinces: Yilgarn Block and Gascoyne Province. In: Recognition of Uranium Provinces 1989, pp. 273–304. International Atomic Energy Commission, Vienna.
43. Anand, R.R.; Paine, M. Regolith geology of the Yilgarn Craton, Western Australia: implications for exploration. *Aust. J. Earth Sci.* **2002**, *49*, 3–162.
44. Bunting, J.A.; Van de Graaff, W.J.E.; Jackson, M.L. Palaeogeography of the Eastern Goldfields, Gibson Desert and Great Victoria Desert. Geological Survey of Western Australia Annual Report for 1973, 1974, 45–50.
45. Morgan, K.H.; Peers, R. Esperance – Mondrain Island geological sheet, SI51-6 & SI51-10. Geological Survey of Western Australia, 1:250 000 Geological Series Explanatory Notes 1973.
46. Cope, R.N. Tertiary epeirogeny in the southern part of Western Australia. Geological Survey of Western Australia Annual Report for 1974, 1975, pp. 40-46.
47. de Broekert, P., Sandiford, M. Buried inset-valleys in the Eastern Yilgarn Craton, Western Australia: geomorphology, age, and allogenic control. *J. Geol.* **2005**, *113*, 471–493.
48. Finkl, C.W. Stripped (etched) landsurfaces in southern Western Australia. *Aust. Geogr. Stud.* **1979**, *17*, 33–52.
49. Anand, R.R.; Butt, C.R.M. A guide for mineral exploration through the regolith in the Yilgarn Craton, Western Australia. *J. Geol. Soc. Aust.* **2010**, *57*,1015–1114. doi: 10.1080/08120099.2010.522823.
50. Lillicrap, A.M.; Biermann, V.; George, R.J.; Gray, D.J.; Oldham, C.E. The distribution and origins of extremely acidic saline groundwaters in the south of Western Australia - groundwater and digital mapping datasets provide new insights. *J. Hydrol.* **2017**, *556*, 717-731. https://doi.org/10.1016/j.jhydrol. 2017.11.044

51. González-Álvarez, I.; Anand, R.R.; Hough, R.; Salama, W.; Laukamp, C.; Sweetapple, M.T.; Ley-Cooper, Y.; Sonntag, I.; Lintern, M.; Abdat, T.; le Gras, M.; Walshe J. Greenfields geochemical exploration in a regolith-dominated terrain: the Albany–Fraser Orogen/Yilgarn Craton margin: Geological Survey of Western Australia, Report 144, 2014, 213p.
52. Laukamp, C.; Salama, W.; González-Álvarez, I. Proximal and remote spectroscopic characterisation of regolith in the Albany–Fraser Orogen (Western Australia). *Ore Geol. Rev.* **2016**, *73*, 540–554. https://doi.org/10.1016/j.oregeorev.2015.10.003
53. Heavy Rare Earths Ltd. Metallurgical program delivers two-fold grade increase and up to 91.3% extraction of magnet rare earths. Australian Stock Exchange Announcement, 12 July 2023.
54. OD6 Metals; The REE Potential of the Esperance District. ANU REE Conference presentation 16 November 2022. Available online: https://www.od6metals.com.au/wp-content/uploads/2024/05/61180850-2.pdf (accessed on 19 July 2024).
55. 96Rogers, K.A. Esperance project, exploration licences E63/1415, E63/1469, E63/1496, E69/2783, E69/2784 and E69/2944. Combined annual technical report for the period 6 May 2014 to 5 May 2015. Salazar Gold Pty Ltd. 2018, WAMEX A106234, 177p.
56. OD6 Metals; Standout Grades, Thickness and Extent of REE Mineralisation Confirmed at Centre Prospect; Australian Stock Exchange Announcement, 9 November 2023.
57. Meeka Metals; 12m @ 4,276ppm TREO – Further High-Grade Infill and Extensional Assays Support Initial Circle Valley REE Mineral Resource; Australian Stock Exchange Announcement, 9 May 2023.
58. Mount Ridley Mines; Coincident High-Grade Rare Earth Elements and Geophysical Anomalies at Mia Prospect; Australian Stock Exchange Announcement, 10 May 2023.
59. Dundas Minerals; Exploration Update: Rare Earth Elements Exploration Program. Australian Stock Exchange Announcement, 30 May 2023.
60. Rogers, K.A. Esperance project, exploration licences E63/1415, E63/1469, E63/1496, E69/2783, E69/278, E69/2944 and E69/301. Combined annual technical report for the period 6 May 2012 to 5 May 2013. Salazar Gold Pty Ltd. 2013, WAMEX A098490, 102p.
61. Li, Y.H.M.; Zhao, W.W.; Zhou, M.F. Nature of parent rocks, mineralization styles and ore genesis of regolith-hosted REE deposits in South China: an integrated genetic model. *J Asian Earth. Sci.* **2017**, *148*, 65-95.
62. Bao, Z.; Zhao, Z. Geochemistry of mineralization with exchangeable REY in the weathering crusts of granitic rocks in South China. *Ore. Geol. Rev.* **2008**, *33*, 519–535. doi: 10.1016/j.oregeorev.2007.03.005.
63. Braun, J.-J.; Pagel, M.; Muller, J.-P.; Bilong, P.; Michard, A.; Guillet, B. Cerium anomalies in lateritic profiles. *Geochim. Cosmochim. Acta* **1990**, *54*, 781–795.
64. Chi, R.; Tian, J. Review of weathered crust rare earth ores. *J. Chinese Rare Earth Soc.* **2007**, *25*, 641–650 (in Chinese with English abstract).
65. Chi, R.; Tian, J.; Luo, X.; Xu, Z.; He, Z. The basic research on the weathered crust elution-deposited rare earth ores. *Nonferrous Met. Sci. Eng.* **2012**, *3(4)*, 1–13 (in Chinese with English abstract).
66. Sanematsu, K.; Kon, Y.; Imai, A.; Watanabe, K.; Watanabe, Y. Geochemical and mineralogical characteristics of ion-adsorption type REE mineralization in Phuket, Thailand. *Miner. Deposita* **2013**, *48*, 437–451.
67. Townend, R.; Townend, D. Townend mineralogy laboratory report 5 January 2016. In: Rogers, K.A. Esperance project, exploration licences E63/1415, E63/1469, E63/1496, E63/1749, E69/2783, E69/2784 and E69/2944. Combined annual technical report for the period 6 May 2015 to 5 May 2016. Salazar Gold Pty Ltd. 2018, WAMEX A109432, 135p.
68. Rogers, K.A. Esperance project, exploration licences E69/2783 and E69/2784. Final surrender technical report for the period 6 May 2011 to 5 April 2018. Salazar Gold Pty Ltd., 2018; WAMEX A117039, 62p.
69. Foley, N.; Ayuso, R. REE enrichment in granite-derived regolith deposits of the Southeastern United States: Prospective source rocks and accumulation processes. In Symposium on Strategic and Critical Materials Proceedings, November 13-14, 2015, Victoria, British Columbia; Simandl, G.J., Neetz, M., Eds ; British Columbia Ministry of Energy and Mines, 2015, British Columbia Geological Survey Paper 2015-3, pp 131-138.
70. Townend, R. Roger Townend and Associates Consulting Mineralogists report 28/10/2011. In: Rogers, K.A. Esperance project, exploration licences E63/1415, E63/1469, E63/1496, E63/1749, E69/2783, E69/2784, E69/2944 and E69/3010. Combined annual technical report for the period 6/5/2012 to 5/4/2013. Salazar Gold Pty Ltd. 2013, WAMEX A098490, 102p.
71. Townend, R.; Townend, D. Townend mineralogy laboratory report RT23634, 8 April 2014, 29p.
72. Chi, R.; Tian, J. Weathered Crust Elution-Deposited Rare Earth Ores, Nova Science Publishers, 2009, New York, 288p.
73. Denys, A.; Janots, E.; Auzende, A.L.; Lanson, M.; Findling, N.; Trcera, N. Evaluation of selectivity of sequential extraction procedure applied to REE speciation in laterite. Chem. Geol. 2021, 559, 119954. https://doi.org/10.1016/j.chemgeo.2020.119954.

74. Fu, W.; Li, X.T.; Feng, Y.Y.; Feng, M.; Peng, Z.; Yu, H.X.; Lin, H. Chemical weathering of S-type granite and formation of rare earth element (REE)-rich regolith in South China: critical control of lithology. *Chem. Geol.* **2019**, *520*, 33–51.
75. Li, M.Y.H.; Zhou, M.F.; Williams-Jones, A.E. The genesis of regolith-hosted heavy rare earth element deposits: Insights from the world-class Zudong deposit in Jiangxi Province, South China. *Econ. Geol.* **2019**, *114*, 541–568.
76. Sanematsu K.; Kon Y. Geochemical characteristics determined by multiple extraction from ion- adsorption type REE ores in Dingnan County of Jiangxi Province, South China. *Bull. Geol. Surv. Japan* **2013**, *64*, 313-330, https://doi.org/10.9795/bullgsj.64.313.
77. Wenzel, W.W.; Kirchbaumer, N.; Prohaska, T.; Stingeder, G.; Lombi, E.; Adriano, D.C. Arsenic fractionation in soils using an improved sequential extraction procedure: *Anal. Chim. Acta.* **2001**, *436*, 309–323.
78. Marquis, E. Rare earth element (REE) mobility in alkaline igneous rocks and the potential impact on the formation of ion adsorption type REE ores of the Ambohimirahavavy alkaline complex. PhD Thesis, the University of Brighton, UK, 19 September 2019.
79. Sanematsu, K.; Ejima, T.; Kon, Y.; Manaka, T.; Zaw, K.; Morita, S.; Seo, Y. Fractionation of rare-earth elements during magmatic differentiation and weathering of calc-alkaline granites in southern Myanmar. *Mineral. Mag*. **2016**, *80(1)*, 77-102. https://doi.org/10.1180/minmag.2016.080.053
80. Li, M.Y.H.; Kwong, H.T.; Williams-Jones, A.E.; Zhou, M.-F. The thermodynamics of rare earth element liberation, mobilization and supergene enrichment during groundwater-regolith interaction. *Geochim. Cosmochim. Acta* **2022**, *330*, 258-277.
81. Chi, R.A.; Tian, J. *Weathered crust elution-deposited rare earth ores*; Nova Science Publishers: New York, USA, 2008, 288 p.
82. Marker, A.; de Oliveira, J.J. Climatic and morphological control of rare earth distribution in weathering mantles on alkaline rocks. *Catena* 1**994**, *21*, 179–193.
83. Li, M.Y.H.; Zhou, M.-F.; Williams-Jones, A.E. Controls on the dynamics of rare earth elements during sub-tropical hillslope processes and formation of regolith-hosted deposits. *Econ. Geol.* **2020**, *115*, 1097-1118.
84. Wang, M.; Li, M.Y.H., Zhou, M.-F.; Zhou, J.-X.; Sun, G.; Xiao, S.; Liu, F.-X.; Zhang, Z.-J. Enrichment of rare earth elements in weathered alkaline igneous systems: Insights from the Puxiong regolith-hosted REE deposit, SW China. *Econ. Geol.* **2024**, *119*, 161-187.
85. Freyssinet, Ph. Ore-forming processes related to lateritic weathering. *Econ. Geol.* **2005**, *100th anniversary issue*, 681-722.
86. Samama, J.-C. *Ore Fields and Continental Weathering*. Van Nostrand Reinhold Company: New York, USA, 1986.
87. González-Álvarez, I.; Salama, W.; Anand, R.R. Sea-level changes and buried islands in a complex coastal palaeolandscape in the South of Western Australia: Implications for greenfield mineral exploration, *Ore Geol. Re.* **2016**, *73*, 475-499, ISSN 0169-1368, https://doi.org/10.1016/j.oregeorev.2015.10.002.
88. Bird, M.I.; Chivas, A.R. Stable-isotope geochronology of the Australian regolith. *Geochim. Cosmochim. Acta* **1989**, *53*, 3239–3256.
89. Clarke, J.D.A. Evolution of the Lefroy and Cowan palaeodrainage channels, Western Australia. *Aust. J. Earth Sci.* **1994**, *41*, 55–68.
90. Dammer, D.; McDougall, I.; Chivas, A.R. Timing of weathering-induced alteration of manganese deposits in Western Australia: evidence from K/Ar and 40Ar/39Ar dating. *Econ. Geol.* **1999**, *94*, 87–108.
91. Long, D.T.; Lyons, W.B.; Hines, M.E. Influence of hydrogeology, microbiology and landscape history on the geochemistry of acid hypersaline waters, N.W.Victoria. *Appl. Geochem.* **2009**, *24*, 285-296.
92. Bowen, B.B.; Benison, K.C. Geochemical characteristics of naturally acid and alkaline saline lakes in southern Western Australia. *Appl. Geochem.* **2009**, *24*, 268-284.
93. Gray, D.J. Hydrogeochemistry in the Yilgarn Craton. *Geochem. Explor. Environ. Anal.* **2001**, *1*, 253-264.
94. Mann, A.W. Hydrogeochemistry and weathering on the Yilgarn Block, Western Australia—ferrolysis and heavy metals in continental brines. *Geochim. Cosmochim. Acta* **1983**, *47*, 181-190.
95. McArthur, J.M.; Turner, J.V.; Lyons, W.B.; Osborn, A.O.; Thirlwall, M.F. Hydrochemistry on the Yilgarn Block, Western Australia: ferrolysis and mineralisation in acidic brines. *Geochim. Cosmochim. Acta* **1991**, *55*, 1273-1288.
96. Bird, M.I.; Andrew, A.S.; Chivas, A.R.; Lock, D.E. An isotopic study of surficial alunite in Australia: 1. Hydrogen and sulphur isotopes. *Geochim. Cosmochim. Acta* **1989**, *53*, 3223-3237.
97. Chivas, A.R.; Andrews, A.S.; Lyons, W.B.; Bird, M.I.; Donnelly, T.H. Isotopic constraints on the origin of salts in Australian playas. 1. Sulphur. *Palaeogeogr. Palaeoclimatol. Palaeoecol.* **1991**, *84*, 309-332.
98. Dickson, B.L.; Giblin, A.M. Features of acid–saline systems of Southern Australia. *Appl. Geochem.* **2009**, *24*, 297-302.
99. Gardner, W.K.; Fawcett, J.D.; Fitzpatrick, R.W.; Norton, R.M. Chemical reduction causing land degradation. I: Overview. *Plant Soil* **2004**, *267*, 51-59.

100. Herczeg, A.L.; Barnes, C.J.; Macumber, P.G.; Olley, J.M. A stable isotope investigation of groundwater-surface water interactions at Lake Tyrrell, Victoria, Australia. *Chem. Geol.* **1992**, *96*, 19-32.
101. Gray, D.J.; Noble, R.R.P. Recent advances in hydrogeochemistry. In: Fitzpatrick, R.W.; Shand, P. (Eds.), Regolith 2006: Consolidation and dispersion of ideas. Proceedings of the CRC LEME Regolith Symposium. Cooperative Research Centre for Landscape Environments and Mineral Exploration, 2006, 109-112.
102. Peiffer, S.; Oldham, C.E.; Salmon, U.; Lillicrap, A.M.; Kusel, K. Does iron cycling trigger generation of acidity in groundwaters of Western Australia? *Environ. Sci. Tech.* **2009**, *43*, 6548-6552.
103. Lillicrap, A; George, R J. The distribution and origins of acid groundwaters in the South West Agricultural Area. Department of Agriculture and Food, Western Australia, Perth. Report 362, 2010.
104. Goldstein, S.J.; Jacobsen, S.B. Rare earth elements in river waters. *Earth Planet. Sci. Lett.* **1988**, *89*, 35 – 47.
105. German, C.R.; Elderfield, H. Rare earth elements in Saanich Inlet, British Columbia, a seasonally anoxic basin. *Geochim. Cosmochim. Acta* **1989**, *53*, 2561 – 2571.
106. Dia, A.; Gruau, G.; Olivie-Lauquet, G.; Riou, C.; Moleńat, J.; Curmi, P. The distribution of rare earth elements in groundwaters: Assessing the role of source-rock composition, redox changes and colloidal particles. *Geochim. Cosmochim. Acta* **2000**, *64*, 4131−4151.
107. Tang, J.; Johannesson, K.H. Speciation of rare earth elements in natural terrestrial waters: assessing the role of dissolved organic matter from the modeling approach. *Geochim. Cosmochim. Acta* **2003**, *67*, 2321 – 2339.
108. Quinn, K.A.; Byrne, R.H.; Schijf, J. Comparative scavenging of yttrium and the rare earth elements in seawater: competitive influences of solution and surface chemistry. *Aquat. Geochem.* **2004**, *10*, 59 – 80.
109. Tang, J.; Johannesson, K. H. Controls on the geochemistry of rare earth elements along a groundwater flow path in the Carrizo Sand aquifer, Texas, USA. *Chem. Geol.* **2006**, *225 (1−2)*, 156−171.
110. Noack, C.W.; Dzombak, D.A.; Karamalidis A.K. Rare Earth Element Distributions and Trends in Natural Waters with a Focus on Groundwater. *Environ. Sci. Tech.* **2014**, *48*, 4317-4326. DOI: 10.1021/es4053895
111. Welch S.A., Christy A.G., Isaacson L and Kirste D. Mineralogical control of rare earth elements in acid sulfate soils. *Geochimica et Cosmochimica Acta* **2009**, *73*, 44-64.
112. Fernandez-Caliani, J.C.; Barba-Brioso, C.; de la Rosa, J.D. Mobility and speciation of rare earth elements in acid minesoils and geochemical implications for river waters in the southern Iberian margin. *Geoderma* **2009**, *149*, 393-401.
113. Merten, D.; Geletneky, J.; Bergman, H.; Haferburg, G.; Kothe, E.; Büchel, G. Rare Earth patterns: A tool for understanding processes in remediation of acid mine drainage. *Chem. Erde.* **2005**, *65*, 97-114.
114. da Silva, E.; Ferreira, E.; Bobos, I.; Matos, J.; Patinha, C.; Reis, A.P.; Fonseca, E.C. Mineralogy and geochemistry of trace metals and REE in massive volcanic sulphide host rocks, stream sediments, stream waters and acid mine drainage from the Lousal mine area (Iberian Pyrite Belt, Portugal). *Appl. Geochem.* **2009**, *24*, 383-401.
115. Sahoo, P.K.; Tripathy, S.; Equeeniddin, S.M.; Panigrahi, M.K. Geochemical characteristics of coal mine discharge vis-à-vis behaviour of rare earth elements at Jaintia Hills coalfield, northeastern India. *J. Geochem. Explor.* **2012**, *112*, 235-246.
116. Borrego, J.; Carro, B.; Lopez-Gonzalez, N.; de la Rosa, J.; Grande, J.; Gomez, T.; de la Torre, M. Effect of acid mine drainage on dissolved rare earth elements geochemistry along a fluvial-estuarine system: The Tinto−Odiel Estuary (SW Spain). *Hydrol. Res.* **2012**, *43* (3), 262−274.
117. Ayora, C.; Macías, F.; Torres, E.; Nieto, J.M. Rare Earth Elements in Acid Mine Drainage. Rare Earth Elements in Acid Mine Drainage 2015. XXXV Reunión de la Sociedad Española de Mineralogía Huelva 30 de junio al 3 de julio de 2015, 1-22.
118. Gray, D. J. Hydrogeochemistry in the Yilgarn Craton. CSIRO Division of Exploration and Mining, Perth, Restricted Report 312R, 1996 (Reissued as Open File Report 99, CRC LEME, Perth, 2001).
119. Kim, E.; Osseo-Asare, K. Aqueous stability of thorium and rare earth metals in monazite hydrometallurgy: Eh–pH diagrams for the systems Th–, Ce–, La–, Nd– (PO_4)–(SO_4)–H_2O at 25°C. *Hydrometallurgy* **2012**, *113–114*, 67-78. ISSN 0304-386X, https://doi.org/10.1016/j.hydromet.2011.12.007.
120. Shuai, G.; Zhao, L.; Wang, L.; Dali Cui, Z-L. Aqueous stability of rare earth and thorium elements during hydrochloric acid leaching of roasted bastnaesite. *J. Rare Earth.* **2017**, *35*, 12, 1255-1260. ISSN 1002-0721, https://doi.org/10.1016/j.jre.2017.06.007.
121. Butt, C.R.M.; Horwitz, R. C.; Mann, A. W. Uranium occurrences in calcretes and associated sediments in Western Australia. CSIRO, Div. of Mineralogy Report FP 16, 1977, 66 p.